R. & M. No. 3511

MINISTRY OF TECHNOLOGY

AERONAUTICAL RESEARCH COUNCIL

REPORTS AND MEMORANDA

Air Condensation Effects Measured in the R.A.E. 7 in. x 7 in. Hypersonic Wind Tunnel

By J. F. W. Crane and R. J. Marshall

LONDON: HER MAJESTY'S STATIONERY OFFICE

1968

PRICE 17*s.* 6*d.* NET

Air Condensation Effects Measured in the R.A.E. 7 in. x 7 in. Hypersonic Wind Tunnel

By J. F. W. Crane and R. J. Marshall

Reports and Memoranda No. 3511*
April, 1966

Summary.

It is important to study the effects of air condensation in hypersonic wind tunnels and to establish the degree of supersaturation achievable because savings in heating requirements or increase in Mach number may be achieved. The degree of supersaturation measured in this tunnel shows that with the present heater the upper limit on Mach number may be extended[22] from $M = 9$ to $M = 12$.

Proof testing of models is required to establish that results in supersaturated flow agree with those obtained in subsaturated flow because localised condensation effects in expansion regions may occur. Integrated pressure distributions on a Nonweiler wing show that sub- and super-saturated flows give similar results but that condensing flow shows differences in $\bar{c}_p$ on the suction side at low incidence and on the windward side at high incidence, which results in a decrease in L/D_{max} without friction of about 10 per cent.

LIST OF CONTENTS

*Replaces R.A.E. Tech. Report No. 66 137—A.R.C. 28 319.

LIST OF CONTENTS—*continued*

---

1. *Introduction.*

This Report describes the work done on the effects of air condensation on the flow in the R.A.E. 7 in. × 7 in. hypersonic wind tunnel[1]. Some of this work was described in a paper presented at the 1965 meeting of the Supersonic Tunnels Association in the U.S.A. A more detailed analysis is now presented with the addition of work done earlier at $M = 6{\cdot}8$ by R. J. Marshall and some measurements on a Nonweiler[2] wing.

Work on air condensation in nozzles has been stimulated by the demand for hypersonic Mach-number testing facilities. When air is accelerated through a nozzle the stream temperature falls due to the conversion of enthalpy (heat energy) to velocity energy, and for a Mach number of about five it becomes necessary to preheat the air to avoid condensation. The Mollier diagram, Fig. 1a, describes an isentropic expansion from point 1 to point 2 on the saturated-vapour line. Beyond this line the air should start to condense. The condensation line obtained from calorimeter measurements is described by the equation in Fig. 1b and it has been wind-tunnel practice to avoid crossing this line. This means that air must be preheated to a high temperature to obtain the large expansions demanded by high Mach number.

However, it has been found that in fast expansions, such as occur in wind tunnels, some supersaturation i.e. crossing of the condensation line without condensation, may be obtained. If significant amounts of supersaturation are achievable then very worthwhile savings in stagnation temperature and some increase in Reynolds number accrue. Conversely, higher Mach numbers may be achieved for the same heating.

2. *Argument for Supersaturation.*

The relationship between vapour pressure and temperature for a liquid having a surface of large radius is given by the Clapeyron-Clausius equation:

$$\frac{dp}{p} = -\frac{L}{RT^2}dT$$

or

$$\log_e p = -\frac{L}{RT} + \text{a constant}$$

where p is the pressure, L is the latent heat of vaporisation, R is the gas constant, and T is the temperature. This equation is used to relate the steady-state measurement of vapour pressure and temperature obtained by calorimeter[10] as in Fig. 1b. Vapour pressure is related to surface tension by the equation:

$$p_1 - p_2 = 2\sigma/r$$

where p_1 is the pressure inside a droplet, p_2 is the external pressure, r is the droplet radius, and σ is the surface tension.

Lord Kelvin[3] showed that vapour pressure p_r in a fog containing droplets of radius r is given by the equation:

$$\log_e \frac{p_r}{p_\infty} = 2\sigma/r\rho RT$$

where ρ is the density of the droplet and p_∞ is the vapour pressure for a flat surface. Hence for a given pressure and temperature only one size of droplet is in equilibrium; oversize drops will grow; undersize drops will evaporate.

The idea of supersaturation was advanced in 1880 by Maxwell[3]. The degree of supersaturation is defined as:

$$\frac{\text{DENSITY OF SUPERCOOLED VAPOUR}}{\text{DENSITY OF SATURATED VAPOUR AT THE SUPERCOOLED TEMPERATURE}}$$

Condensation is said to occur heterogeneously if the nuclei which are essential to the process are supplied by other material. It is said to occur homogeneously if the nuclei are provided by the process of self-nucleation. An idea of the extremely small size of particle produced in the latter process is given by Thomann[4] who has shown that when water vapour in air is expanded rapidly in a wind tunnel, in spite of the presence of dust particles, the nuclei produced homogeneously, deduced from theory, were composed of 3 or 4 molecules. In the ensuing condensation these particles grew to a size of about 300 molecules ($r = 14$ Å). For a range of absolute humidity up to 0·002 this particle size was constant.

Wilson[3] showed that in a cloud chamber in the absence of dust particles condensation did not occur with wet air until a considerable supersaturation was reached. When the degree of supersaturation reached $p_r/p_\infty = 8$, a cloud appeared almost instantaneously throughout the mixture.

Supersaturation of air in a nozzle expansion has been observed by various workers for example Grey and Nagamatsu[5] at $M = 6$ and 8·9. The effect of impurities on the supersaturation of nitrogen in a nozzle was studied by Arthur and Nagamatsu[6]. They found that CO_2 and H_2O had a marked effect but if their quantities were less than 0·0001 of the volume the degree of supersaturation of nitrogen was not affected. The effect of oxygen and argon was small; the addition of 23 per cent oxygen reducing the supercooling from 23 deg C to 15 deg C.

Daum[7] has shown that at low pressure ($p < 0{\cdot}1$ mm Hg) air can be cooled by similar amounts in fast expansions in wind tunnels. He and Gyarmathy[8] have shown that these results at low pressure follow the theoretical curves for nitrogen predicted by a spontaneous nucleation theory. At higher pressures most wind-tunnel results show smaller degrees of supercooling and this they attribute to the effect of impurities such as CO_2 and H_2O in the flows causing some heterogeneous condensation.

A saturated expansion theory (S.E.T.) has been proposed by Buhler[5] which serves as a useful reference to the behaviour of pressure and to g the fraction of condensate in condensing flows.

3. *Description of Wind Tunnel.*

The tunnel was a blow-down type, non return, with a 7 inch square working section. Moisture was extracted from the air supply in the normal process of compressing it to 3000 p.s.i. and cooling to a temperature of about 5 deg C for storage. Measurement of humidity[18] showed that the water content of the stored air was always less than 30 parts per million by weight. Oil contamination and hence CO_2 from combustion products was considered to be extremely small judging by the clean condition of the walls of the high pressure pipework at the heater entry. Some oil vapour must have been present in minute quantities, however, in the absence of a direct measure of the air composition the normal composition of air[21] given in Table 3 may be assumed. Dust was filtered by screens of sintered wire gauze of very fine mesh size.

Fig. 2 shows sketches of the two contoured nozzles used, one is two-dimensional for $M = 6{\cdot}8$, the other is axisymmetric for $M = 8{\cdot}6$. The construction of the latter has not been described in previous reports and is perhaps worthy of some mention. It was made from a forging of S56 material, a steel with a low nickel and chromium content having a high strength at 600 deg C. The working profile is continuous from the nozzle exit to a point 1·5 inches upstream of the throat. At this point there is a gap to accommodate thermal expansion of the thin throat section. This section has to absorb high heat transfer rates at the start of a run, when the nozzle walls are cold. The wall thickness was reduced to 0·05 inches in this region to minimise the thermal stress and to allow a quick warm up, thus stabilising the throat area and hence tunnel Mach number. The throat section is faired by a radius into the nozzle block to minimise stress concentration at the junction. The nozzle ordinates[9] are compensated for thermal expansion to a temperature of 600 deg C in the throat region and are uncorrected elsewhere.

4. *Probes and Instrumentation.*

4.1. *Composite Probe.*

A composite probe consisting of a pitot tube, a cone/cylinder static pressure tube, and thermocouples is shown in Fig. 3. The static tube had 4 holes at 90 deg leading to a common reservoir. The holes were free from burrs and other edge effects which could cause errors (*see* Appendix B). The thermocouples were made of Chromel/Alumel wires of 0·005 inch diameter and were welded to form spherical beads of 0·021 inch diameter. Each bead was positioned at the leading edge of an asbestos (Sindanyo) plate and the wires were glued to the surface with a high-temperature strain-gauge cement (Brimor). Two leading edge thicknesses were used, namely sharp and blunt. The blunt leading edge produced a bow shockwave which stood-off 0·04 inches from the thermocouple bead, and this thermocouple attained the higher level of recovery factor Fig. 11, ranging in value from 0·94 to 0·995 according to conditions.

The sharp-edge thermocouple was similarly attached and in this case the bead produced its own shockwave which had a stand-off distance of about 0·0015 inch. It was hoped that in consequence of the small stand-off distance that this probe would be sensitive to the presence of condensate particles, since

the distance in which re-evaporation must occur in order to have no effect on the measured temperature is extremely small. The results support this reasoning. This probe had a recovery factor of 0·91 to 0·94 according to conditions.

4.2. *Settling Chamber Temperature Probe.*

The temperature in the settling chamber, T_0, was measured with a single thermocouple, depicted in Fig. 4. This had a quick response. Previous calibration had shown that the spatial temperature distribution had an average variation of 2 deg C and that single point monitoring of temperature was adequate. (All temperatures were measured within an inch of the tunnel centreline and were recorded on a digital voltmeter.)

Accuracy of temperature measurement was ± 1 deg C.

4.3. *Pitot Rakes.*

Two pitot rakes (not drawn) were used to obtain spatial surveys of the flow. Pitot tubes with square-cut ends were $1\frac{1}{2}$ mm *O.D.*, 1 mm *I.D.* for the radial survey rake, Fig. 21, and 2 mm *O.D.*, $1\frac{1}{2}$ mm *I.D.* for the longitudinal survey rake Figs. 14, 15, 16.

4.4. *Static Pressure Rake.*

Fig. 5 gives details of the construction of this rake. All holes were carefully made to avoid edge defects. In use an unusually high pressure was measured with the central tube. The reason for this is explained in Appendix A. Displacement effects *etc.* caused all tubes to indicate pressures above true static pressure (*see* Appendix B).

4.5. *Manometers.*

Silicone-oil manometers were used to measure static pressure because with the low density of oil the sensitivity is more than ten times that of a mercury manometer. A mercury manometer and a capsule manometer[1] (Midwood) were used to measure pitot pressure, since this is considerably bigger and hence easier to measure than static pressure. All manometers were referred to a near vacuum which was measured absolutely by a type of McLeod gague (Vacustat).

4.6. *Stagnation-pressure Rig.*

Stagnation pressure p_0, was measured[1] at the settling chamber using a transducer of ± 25 p.s.i. range which was referred to a known high pressure. The latter was measured by a deadweight testing machine. The transducer output was recorded on a chart. The accuracy of measurement of p_0 was 0·1 per cent.

5. *Results at* $M = 6{\cdot}8$.

5.1. *Test Technique.*

These results were the first to be obtained on air condensation in this wind tunnel and were privately reported by R. J. Marshall. Only the more important parts of this work are described now.

In these tests the composite probe but without the sharp-edge thermocouple was used, and measurements were made at a single station 41·75 inches downstream of the throat. Runs lasting a minute or so were made which allowed for the slow response of the static pressure probe. At the appropriate time the manometers were clamped, the temperatures were recorded and the airflow was stopped. Manometers were then read and the stagnation pressure deduced from the chart record.

5.2. *Variation of Pitot and Static Pressure with Temperature.*

Fig. 6 shows plots of the variation of pitot pressure p'_0 and static pressure p with stagnation temperature T_0 at $p_0 = 300$ p.s.i.g. Calculated profiles from the Saturated Expansion Theory (S.E.T.) of Buhler[5] are also drawn assuming a constant test section to throat area ratio $A/A^* = 92{\cdot}19$. This theory assumes isentropic expansion (1 to 2, Fig. 1a) to the saturation line followed by expansion (2 to 4) along the line. The latter is described[10] by the equation in Fig. 1b.

At this pressure level the Mach number from p'_0/p_0 for subsaturated flow was $M = 6{\cdot}81$. Static pressure was obtained from the Mach number relationship, and T_{cc} the saturation temperature at this pressure

was obtained from the Clapeyron-Clausius equation. Hence $(T_0)_{cc}$ (the stagnation temperature as predicted from the Clapeyron-Clausius definition of condensation onset) was obtained from the equation $(T_0)_{cc} = T_{cc}(1+\frac{\gamma-1}{2}M^2)$.

The pitot-pressure profile exhibits a trough at the onset of condensation, which because of the sparseness of data points, was inferred from the subsequent profiles for $M = 8{\cdot}6$. Condensation onset was taken as the 1st peak in the profile prior to the trough. As the temperature is reduced the 2nd peak in the profile is observed followed by a steady fall in pressure with reduction in temperature. The S.E.T. predicts a gradual increase in pitot pressure with condensation.

The static pressure increases with reduction in temperature below condensation onset. The latter is delayed by 50 deg C, on the T_0 scale, beyond that predicted by the Clapeyron-Clausius equation. The S.E.T. describes a faster rate of increase in pressure with reduction in temperature. These results show that at this pressure level some supersaturation is occurring. The results at higher pressure levels show similar trends but the amounts of supersaturation are less.

5.3. *Variation of Shockwave Angle with Temperature.*

Fig. 9 shows the variation in angle of the shockwave from the tip of the static-pressure probe of Fig. 3 with temperature. Direct shadow pictures were taken with parallel light at constant normal angle to the flow. The tip shockwave was only just discernible and the angle θ was determined by measurement of the distance between the shock and the probe centreline at a point 7 cm from the probe tip. This angle is therefore intermediate between the cone shockwave angle and the shock angle downstream of the influence of the expansion at the cone/cylinder junction. All the angles measured were greater than would be expected for the cone in inviscid flow and of course were greater than the Mach angle.

The angle θ decreases steadily with reduction in temperature in the sub and super saturated regimes, due not to the variation in Mach number indicated by pitot but to a reduction in boundary-layer displacement caused by an increase in Reynolds number. At $T_0 = 562$ deg K the minimum angle is attained; below this temperature the angle increases due to condensation. The S.E.T. shows that condensation causes a decrease in Mach number and these results, although masked by boundary-layer displacement effect support this reasoning. The important conclusion to be drawn is that the minimum wave angle occurs at about the same temperature as that indicated by a pitot tube for condensation onset.

6. *Results at $M = 8{\cdot}6$.*

6.1. *Test Technique.*

A much more detailed series of tests was made with the axisymmetric nozzle at $M = 8{\cdot}6$. For this series the run length was standardised at 80 seconds to ensure that the probes exhibited constant response and recovery factors, and to ensure that the tunnel wall boundary layer, whose thickness is dependent on wall temperature, would not influence the measurements. Runs were made in the order of decreasing pressure.

6.2. *The Joule-Thomson Effect on Total Temperature.*

With reference to the Mollier diagram, Fig. 1a it may be seen that isotherms are not parallel to isenthalps. Hence in an adiabatic expansion 1–2–5 from stagnation conditions at high pressure to stagnation conditions at low pressure, such as occurs in throttling, the stagnation enthalpy is constant but the temperature is changed. This temperature change ΔT is known as the Joule-Thomson[3] effect and the slope $\Delta T/\Delta P$ is known as the Joule-Thomson coefficient. The energy equation for a steady adiabatic flow of a gas at constant altitude states that enthalpy plus kinetic energy is a constant. Therefore in a nozzle flow of this type the stagnation enthalpy upstream of the throat is equal to the stagnation enthalpy downstream of a normal shock downstream of the throat. Using tables [11] the change in total temperature, ΔT, to be expected in expanding air down to one atmosphere was calculated, Fig. 10. (Futher expansion produces negligible change in temperature.) At temperatures below 600 deg K ΔT is negative and in the range 620 to 900 deg K ΔT is positive. From this information curves for maximum recovery factor, T'_0/T_0, are drawn in the following figures.

6.3. *The Variation of Thermocouple-probe Recovery Factors with Temperature.*

Fig. 11 shows the variation of recovery factor of both probes with time and Reynolds number at a temperature of 690 to 850 deg K. Recovery factor increases with immersion time and with increase in Reynolds number. Both probes are below the theoretical maximum recovery factor but the blunt-edge probe has the superior recovery.

Fig. 12 shows the variation of recovery factor of both probes with temperature for constant immersion times of 80 sec. At $p_o = 300$ p.s.i.g., Fig. 12a, the sharp-edge probe shows condensation onset at $(T_0)_{t/c}$ the total temperature for condensation onset indicated by thermocouple = 595 deg K shown by the rapid drop in T'_0/T_0 from 0·922 to 0·79 at $T_0 = 380$ deg K. At lower temperatures the recovery factor begins to rise again. The theoretical saturation temperature is $(T_0)_{cc} = 772$ deg K which indicates that condensation is considerably delayed at this pressure. Since in the process of condensation latent heat is given up to the surrounding gas the recovery factor measured by a thermocouple in condensing flow would be greater than that measured in sub or super saturated flow if no re-evaporation occurred. But if re-evaporation occurred rapidly enough downstream of the shockwave the thermocouple would be unaffected by condensation. However, in the third case, for re-evaporation at the thermocouple, there is a reduction in recovery factor and this is the effect produced on the sharp-edge thermocouple. The second case describes the effect on the blunt-edge thermocouple. At somewhat lower temperatures the pictures change, the blunt-edge thermocouple becomes sensitive to condensation and the sharp-edge thermocouple becomes less sensitive. This indicates a greater penetrating power of the condensate particles, i.e. they have become larger.

Fig. 12b shows similar plots for $p_0 = 500$ p.s.i.g. and at this pressure level the recovery factors are slightly higher, 0·973 for the blunt-edge thermocouple and 0·933 for the sharp-edge thermocouple, without condensation. Condensation onset is at $(T_0)_{t/c} = 653$ deg K, indicated by the sharp-edge probe and at this temperature the blunt-edge probe is affected by condensation very slightly. This indicates a big delay in condensation since $(T_0)_{cc} = 794$ deg K. The recovery factor of the sharp-edge probe drops to a minimum of 0·76 at $T_0 = 420$ deg K and then rises as before at the lower temperatures. The blunt-edge probe has a constant recovery factor of 0·964 from condensation onset until $T_0 = 460$ deg K after which it drops steadily to 0·915 at $T_0 = 300$ deg K.

Fig. 12c, for $p_0 = 750$ p.s.i.g. shows subsaturated recovery factors of 0·989 for the blunt-edge probe and 0·94 for the sharp-edge probe. Both probes indicate condensation onset at $T_0 = 685$ deg K compared with $(T_0)_{cc} = 820$ deg K. The recovery factor for the sharp-edge probe drops to a minimum of 0·75 at $T_0 = 410$ deg K then rises to 0·78 at $T_0 = 300$ deg K. The recovery factor for the blunt-edge probe remains constant at 0·964 in the condensing region down to $T_0 = 420$ deg K and then drops to 0·91 at $T_0 = 300$ deg K.

Summarising, the sharp-edge probe gave a good indication of condensation onset at all pressure levels, shown by a drop in recovery factor caused by the cooling effect of re-evaporation of the condensed particles at the bead surface. The blunt-edge thermocouple probe was insensitive to condensation onset at the lower pressure levels and only slightly sensitive to it at the highest pressure level. A rapid increase in particle size was indicated by a decrease in the rate of evaporation at the bead of the sharp-edge probe and a corresponding increase at the bead of the blunt-edge probe at $T_0 \simeq 420$ deg K.

6.4. *Static-pressure distribution.*

Fig. 13 shows the distribution of static pressure measured with the rake, Fig. 5, in subsaturated flow. The profile across the core is reasonably uniform; the pressures at $r = 3$ and 3·5 inches are low because they are in the expansion region, from round nozzle to square working section. The pressure level is somewhat higher than theoretical due to displacement effects of the probe (*see* Appendix B).

The longitudinal distribution reveals a slightly expanding flow.

6.5. *Pitot-pressure Distribution.*

Traverses with a 5 tube pitot rake, with tubes one inch apart, were made along the nozzle for subsaturated flow, Fig. 14, slightly supersaturated flow, Fig. 15, and condensing flow, Fig. 16. Fig. 14 and 16 are for $p_0 = 750$ p.s.i.g. and Fig. 15 is for $p_0 = 300$ p.s.i.g. Mach number was obtained from flow tables[12]

and the ratio p'_0/p_0 so that the condensing flow results are given as indicated Mach number and not true Mach number. Each figure shows 3 plots, the 2 lower plots show pitot pressure and Mach number along the centreline, the other shows M_{av} the average Mach number determined from the readings of the 3 centre tubes of the rake. The tubes at $r = 2$ inches were not included because they were brushing the edge of the boundary layer.

In subsaturated flow, Fig. 14, there is a maximum variation in pitot pressure on the centreline of ± 3 per cent, provided by two weak expansions at 4 and 8 inches upstream of the window C_L. The corresponding Mach number variation is $\pm 0{\cdot}06$. Further downstream in the range -4 to $+3$ inches the Mach number variation is much less and describes a weakly expanding flow. In the upper plot of M_{av} the expansion regions at 4 and 8 inches are much weaker than on the centreline. The average Mach number at the window centreline, the normal axis of rotation of a model, is $M = 8{\cdot}58$ and over a range of ± 4 inches the variation is $\pm 0{\cdot}03$.

In supersaturated flow, but at a much lower pressure, very similar profiles were obtained, Fig. 15. At this pressure the tunnel boundary layer is slightly thicker and consequently the Mach number is slightly lower at $M = 8{\cdot}50 \pm 0{\cdot}03$ over the range ± 4 inches. The expansion regions on the tunnel centreline at 4 and 8 inches are slightly weakened which suggests that their origin is at the nozzle profile.

In condensing flow, Fig. 16, the profiles are somewhat different from the above. There is now a slight compression at 7·5 inches and an expansion at $-2{\cdot}5$ inches. The overall reduction in pitot pressure means a slight increase in indicated Mach number. The weakly expanding flow is replaced by an almost perfectly uniform flow in the middle range of $-1{\cdot}5$ to $+4{\cdot}5$ inches with an average indicated Mach number of 8·62. At the upstream end there is a weak expansion which is confined to the centreline region This is preceded by a compression region which is not confined to the centreline comparing M_{C_L} with M_{av}. At the downstream end there is a stronger expansion region which unlike those in the previous figures is not confined to the centreline and is therefore unrelated. It is probably a condensation effect.

6.6. *Pressure Variation with Temperature.*

The upper plots in Figs. 17, 18, 19 show the variation of pitot pressure on the centreline with T_0 for 3 levels of stagnation pressure. All measurements were made at $t = 80$ sec and the runs were made in the order of decreasing pressure. A Midwood capsule manometer was used to measure pitot pressure.

A very distinct trough in the profile was observed at all pressures. Condensation onset is taken as the upper temperature peak, or 1st peak, and this indication agrees quite well with the thermocouple indication. Peak to peak temperature ranges are 120 deg C at $p_0 = 300$ p.s.i.g., 135 deg C at $p_0 = 500$ p.s.i.g., and 135 deg C at $p_0 = 750$ p.s.i.g. Trough to peak pressure ranges are all equal at about 14 per cent of subsaturated pitot pressure. It is shown in the subsequent analysis that a wave pattern induced by condensation moves upstream as the temperature is lowered and the distinct peaking is the result of the axisymmetric shape of the nozzle which produces a focussing effect.

The reduction in pitot pressure at $T_0 = 300$ deg K is about 20 per cent of subsaturated values. The S.E.T. only weakly describes the variation of pitot pressure with condensation.

The lower plots in the above figures show the variation of static pressure measured with the rake Fig. 5. The results are the average of 2 tubes at $r = 1$ inch. This was done to reduce scatter. At the lowest pressure there is a large degree of scatter and there appears to be little effect of condensation, but this is probably due to the insensitivity of the apparatus at this pressure level (Appendix C). Note the curve of pressure response in Fig. 30 (No. 2) which indicates that at this pressure level $p \simeq 1$ mm *Hg* about 1·5 to 3 min of suction is required. However at the 2 higher pressure levels there is a distinct increase of pressure with condensation the commencement being approximately at the same temperature as that indicated by the thermocouple probe. There appears to be a slight drop in pressure, of about 5 per cent, prior to this increase. The S.E.T. predicts an earlier and much greater rise in pressure. This theory shows that g the fraction of condensate achieved was always less than $g = 0{\cdot}05$.

6.7. *Comparison of Pitot-pressure Variation with Temperature at Two Stations on the Tunnel Centreline.*

Fig. 20 shows the variation of pitot pressure at Station 1 for $p_0 = 750$ p.s.i.g. The profile is similar to that for Station 5 but the 2nd peak is displaced 20 deg C in the direction of higher temperature. Otherwise

the results for constant time follow the profile of Station 5. This means that condensation onset is felt at the same temperature everywhere in the test section downstream of the condensation zone and the latter is probably located on the Mach cone boundary (*see* Section 6.8 and Fig. 22).

The advance of the recompression front by 20 deg C over the 4 inch spacing between the two stations means that this wave system, which is induced by the interaction of the condensation zone with the nozzle wall, moves upstream 0·2 inches per degree centigrade at this small level of condensate.

The traces of pitot-pressure variation during single runs follow fairly closely the fixed time results showing that nozzle-wall heating has a small effect on the flow pattern.

6.8. *Comparison of Pitot-pressure Variation with Temperature at Various Radii at Station* 1.

Fig. 21 for $p_0 = 750$ p.s.i.g. shows the variation of p'_0/p_0 with T_0 at different radii at Station 1. The first peak indicating condensation onset occurs at the same temperature at all radii and is in agreement with $(T_0)_{t/c}$. The trough in the profile is most distinct at $r = 0$ and $r = 0{\cdot}5$ inch but becomes progressively smaller at the larger radii. The recompression region acts on the outer radii at higher temperatures when the amount of condensation and resultant expansion is less. As the recompression field advances upstream towards the pitots at the inner radii it becomes stronger due partly to the greater degree of condensation and partly to focussing by the circular-section nozzle. Analysis of these profiles enables the location of this wavefront to be drawn, Fig. 22. The condensation region is presumed to be located at the intersection of this wavefront with the nozzle wall.

7. *Comparison of R.A.E. Results for Condensation Onset with the Steady-state Line and the Daum Line for Wind Tunnels.*

The results for condensation onset are plotted in Fig. 23. All show some degree of supercooling with a maximum of 10 deg C at the lowest pressure of 1·1 mm *Hg*., and indicate that the Daum line[7] for wind tunnels is somewhat conservative in the range 1 to 10 mm *Hg* for this tunnel. Onset was measured at the 1st peak in the pitot-pressure profile, the initial drop in the recovery temperature of the sharp-edge thermocouple, and the beginning of the increase in static pressure. The results are corrected for the small variation in γ according to the method of the Ames tables[12]. Van der Waal's equation[21] for a thermally imperfect gas give RT thermally perfect/RT thermally imperfect equal to 1·002 at stagnation conditions and 1 at free stream conditions. This effect is therefore ignored in the analysis.

It is interesting to note that the Daum line can be approximated by an isentrope but it would have to be chosen carefully to give correct estimates of supersaturation in a desired pressure range.

8. *Pressure Measurements on a Nonweiler Delta-wing Model.*

The tests described show that in fast expansions to low pressure considerable supersaturation of air is achievable. If a model is tested in supersaturated air, providing that local expansions do not cause condensation at the model, the results obtained should be the same as for subsaturated flow.

Accordingly, at a somewhat later period in time the opportunity was taken of making some pressure measurements on a Nonweiler[2] delta-wing model, Fig. 24. At this stage in the tunnel's history the dust-filter section had broken down and the tunnel air was polluted with some fine dust. Fig. 25 shows plots of the average pressure coefficient for the wing calculated from pressures measured at ten spanwise holes at $\frac{3}{4}$ root chord. No measurement of base pressure was made. On the upper surface (leeward) the supersaturated and subsaturated results agree but the results for condensing flow show higher pressure coefficients at low incidence. At 15 deg incidence all flows show $\bar{c}_p$ to be effectively zero, i.e. pressures are equal to free stream pressure for subsaturated flow.

On the lower surface (windward) the results for sub and supersaturated flows are similar but the results for condensing flow indicate lower $\bar{c}_p$ at the higher incidences. Viscous effects are apparent since all results are greater than predicted by inviscid theory.

Fig. 26 shows the variation in lift: drag ratio L/D calculated from the $\bar{c}_p$ plots and without correction for skin friction or base pressure. The sub and supersaturated results are similar but the results for condensing flow show a drop of about 10 per cent in $(L/D)_{max}$.

9. *Conclusions.*

(1) Indication of condensation onset by different methods, pitot pressure, static pressure, recovery temperature, and shockwave angle showed close agreement.

(2) Condensation onset was detected at the same temperature and pressure at several positions in the test section. It is concluded that condensation onset occurs at the Mach boundary of the test section of a nozzle which is profiled for uniform Mach number, and that as the condensate level increases the condensation zone moves upstream.

(3) The variation of pitot pressure with temperature at a fixed station shows a distinct trough after condensation onset. This is caused by movement upstream of the wave pattern produced by the interaction of the condensation zone with the nozzle wall. This movement upstream at low condensate levels was 0·2 inches per deg C in the $M = 8{\cdot}6$ nozzle. The recompression zone was several inches wide and the condensation zone was somewhat smaller in width.

(4) Static pressure increases with condensation but at condensation onset there appears to be a reduction in pressure of about 5 per cent, but this result is only tentative.

(5) The Saturated Expansion Theory describes the trend of static pressure with condensation, neglecting the delay due to supersaturation, but the measured rate of increase in pressure becomes smaller the lower the pressure.

(6) The Saturated Expansion Theory describes weakly the trend of pitot pressure with condensation, neglecting the delay due to supersaturation, but it does not of course predict the peaking produced by the movement of the recompression-wave system across a fixed pitot tube.

(7) Recovery temperature of the sharp-edge thermocouple probe was strongly affected by condensation because the condensate particles were re-evaporated at the thermocouple bead causing a reduction in recovery factor.

(8) The recovery-factor profile indicates a constant size of condensate particle at condensate levels less than 2 per cent. Above this level the particle size increased rapidly indicated by the upward trend in recovery factor of the sharp-edge probe and downward trend in recovery factor of the blunt-edge probe.

(9) Shockwave-angle variation with temperature showed an increase in angle with condensation but this apparent decrease in Mach number was masked by the displacement effect of the boundary layer on the probe producing the shockwave.

(10) Supersaturation was measured at all pressure levels in the range 1 to 11 mm *Hg* and was greater than predicted by the Daum line for wind tunnels. This latter is, of course, a bounding curve and is conservative.

(11) The composition of the air and so of the available nucleants for heterogeneous condensation was the same throughout. But the supersaturation varied only with pressure, expansion rates being roughly equal for the two nozzles, and the lower the pressure the greater the supersaturation. This means that condensation in fast expansions, however achieved whether heterogeneously or homogeneously, is pressure dependent for a uniform composition.

(12) Integrated pressure distributions on a Nonweiler delta wing show that sub and supersaturated flows give similar results but that condensing flows show differences in $\bar{c}_p$, on the suction side at low incidence and on the windward side at high incidence, which results in a decrease in L/D_{max} without friction.

LIST OF SYMBOLS

$\mathring{A}$	Angstrom unit
A/A^*	Area ratio of nozzle from Mach number
C	Constant
C_L	Lift coefficient
L	Latent heat of vaporisation
L/D	Lift : drag ratio
M	Mach number
R	Gas constant
Re	Reynolds number
S	Reading
T	Temperature
$\bar{c}_p$	Pressure coefficient
g	Condensate fraction
k	Constant
p	Pressure
q	Dynamic pressure
r	Radius
t	Time
u,v,w	Velocity
y	Ordinate
Δ	Increment
α	Incidence
γ	Ratio of specific heats
θ	Shockwave angle
ρ	Density
σ	Surface tension

Suffixes.

1	Inside droplet
2	Outside droplet
0	Stagnation condition
av	Average
cc	Clapeyron-Clausius condition

C_L	Centreline
r	Radius
t/c	Thermocouple indication of condensation onset
∞	Infinite radius or free stream behind normal shock

Prime.

1	Behind normal shock

LIST OF REFERENCES

No.	Author(s)	Title, etc.
1	J. F. W. Crane and L. F. Crabtree	The 7 in. × 7 in. hypersonic wind tunnel at R.A.E. Farnborough. Parts I, II, III ARC CP 590. August 1961.
2	T. Nonweiler	Delta wings of shapes amenable to exact shockwave theory. *Jl. R. Aeronaut. Soc.*, Vol. 67, pp. 39–40. 1963.
3	D. A. Wrangham	*The theory and practice of heat engines.* 2nd Edition 1951. Cambridge Univ. Press.
4	H. Thomann	Determination of the size of ice crystals formed during condensation of water in wind tunnels and of their effect on boundary layers. FFA Report 101, 1964, Stockholm.
5	J. Grey and H. T. Nagamatsu	The effects of air condensation on properties of flow and their measurement in hypersonic wind tunnels. Galcit Memo 8. June 1952.
6	P. D. Arthur and H. T. Nagamatsu	Effects of impurities on the supersaturation of nitrogen in a hypersonic nozzle. Galcit Memo 7. March 1952.
7	F. L. Daum	Air condensation in a hypersonic wind tunnel. *AIAA Journal*, Vol. 1, pp. 1043–1046.
8	F. L. Daum and G. Gyarmathy	Air condensation in a rapidly expanding hypersonic flow. A.R.L. Ohio, U.S.A. *XVI – International Astronautical Congress*, Athens, Greece. September 1965.
9	R. F. Clippinger	Supersonic axially symmetric nozzles. BRL Report 794. December 1951.
10	G. T. Furukawa and R. E. McCoskey	The condensation line of air and the heats of vaporization of oxygen and nitrogen. NACA TN 2969. June 1953.
11	J. Hilenrath and C. W. Beckett *et al*	Tables of thermal properties of gases. NBS Circular 564. 1955.
12	Ames Research Staff	Equations tables and charts for compressible flow. NACA Report 1135. 1953.
13	J. Laufer	Aerodynamic noise in supersonic wind tunnels. *Journal of the Aerospace Sciences*, Vol. 28, pp. 685–692. 1961.
14	R. E. Rayle	Influence of orifice geometry on static pressure measurements. A.S.M.E.–59–A–234. 1959.
15	G. D. Arney, Jr and A. B. Bailey	Addendum to an investigation of the equilibrium pressure along unequally heated tubes. AEDC.–TDR.–188. October 1962.
16	S. Goldstein	A note on the measurement of total head and static pressure in a turbulent stream. *Proc. Roy. Soc.* Vol. 155, p. 570. 1936.

REFERENCES—*continued*

No.	*Author(s)*	*Title, etc.*
17	A. Fage	On the static pressure in fully developed turbulent flow. *Proc. Roy. Soc.* Vol. 155, p. 576, 1936.
18	J. F. W. Crane and J. G. Woodley . .	The 7 in. × 7 in. hypersonic wind tunnel at R.A.E. Farnborough. Part IV measurements of diffuser performance, blockage, starting loads and humidity. ARC CP 663. December 1962.
19	R. Shaw	The influence of hole dimensions on static pressure measurements. *Journal Fluid Mechanics*, Vol. 7. 1960.
20	L. Gaudet	Humidity and scale effect on static pressures measured on the walls of a large supersonic wind tunnel. R.A.E. Tech Report 65074, ARC 27162. March 1965.
21	G. W. Kaye and T. H. Laby . .	*Tables of physical and chemical constants.* Longmans, Green & Co. Ltd. 13th Edition. 1966.
22	J. F. W. Crane and D. H. Peckham . .	Possible modifications to the R.A.E. 7 in. × 7 in. intermittent hypersonic tunnel. R.A.E. Tech Report 65103, ARC 27266. May 1965.

APPENDIX A

Explanation of High Pressure Indicated by the Centre Tube of the Static-pressure Rake in Fig. 5.

An unusually high pressure, about twice that of the other tubes was indicated by the centre tube No. 3 of the static-pressure rake. No leaks in the system were found and previous schlieren examination and pitot calibration of the flow had revealed no non-uniformity to account for it. As mounted, the rake could be moved only in incidence so that adjustment of the static-hole position in the tunnel was made by putting the rake at small incidences of 5 and 10 deg. The pressure measured by the centre tube was reduced progressively as it was moved away from the tunnel centreline and so it was able to describe the profile of static pressure across the core of the flow, Fig. 27.

For a time the explanation of static pressure peaking at the tunnel centreline remained a mystery as other more urgent work proceeded but as soon as practicable some more tests were made. This time the rake was mounted on a sting and could be traversed longitudinally. Traverses showed pressure peaking to occur all along the length of the nozzle thus eliminating the existence of an isolated disturbance. A general effect like this it was thought could be due to the focussing of small disturbances generated in the turbulent boundary layer of the tunnel wall i.e. the pseudo-sound discovered by Laufer[13]. Therefore two one inch wide steel plates were placed across the working section, Fig. 27, to act as shields, and the rake was traversed between them. The profiles obtained, Fig. 27, show that the shields eliminated the pressure peaking but their influence was inexplicable. For example the results for a horizontal rake, when only the centre tube was between the shields, were influenced at an extremely forward position almost in line with the shield leading edge. Therefore pseudo-sound was not the cause of static pressure peaking at the centreline.

The rake was then adjusted by inserting a packing piece to align an adjacent tube with the tunnel centreline. The rake was sprayed with a temperature indicating paint and the flow pattern of the paint was observed. The paint was seen to flow downstream everywhere except forward of the sting/blade joint and over most of the centre tube where it was observed to move upstream, Fig. 28. This tube again indicated a high pressure. Schlieren pictures Fig. 29 and 30 show the region of separated flow caused by this sting interference on the centre tube. The vertical black lines in the pictures are produced by baffle plates in the window pockets. Their role is to minimise the heating of the soda-glass windows.

APPENDIX B

Some Sources of Error in the Measurement of Static Pressure.

Apart from sting interference the measured static pressure could be affected by the following:

Displacement effect.

The probe and its boundary layer cause the flow to be displaced and compressed. If the probe is shaped to expand the flow to balance exactly this compression then true static pressure should be measured but this solution will be right for only a single set of flow conditions and hence it is rarely attempted.

Hole-size effect.

The hole-size effect has been thoroughly investigated in incompressible flows but little has been done in the compressible case. In the former case Rayle has shown that with a 1/32 inch diameter hole the measured pressure is greater by $0{\cdot}0035q$, than the true pressure, where q is the dynamic pressure. On the other hand, Shaw has produced a correlating factor for error based on skin friction at the wall, for incompressible flow. Gaudet has shown that errors in pressure measurements on the wall of a large supersonic tunnel can be explained in part by humidity and the remainder in equal parts by boundary-layer displacement and hole-size effect. The latter was calculated from Shaw's empirical relationship using values of density and viscosity evaluated at the wall.

Similar calculations for the present results show that hole-size effect according to Shaw is zero. Rayle, on the other hand predicts $\Delta p = 0{\cdot}0021q$. The latter would account for about 1/3 of the error indicated in Table 2. Boundary-layer displacement, using flat-plate formulae for a weak interaction accounts for about a third and the remainder could be distributed among probe displacement, turbulence and system lags.

Hole-shape effect.

Rayle has shown for incompressible flow that the edge of the hole can produce an effect on pressure measurement. A burr might produce a positive error of $0{\cdot}011q$, an edge radius of $0{\cdot}25d$ might produce an error of $0{\cdot}002q$, and a hole inclined 30 deg to the stream might be in error by $0{\cdot}003q$. A countersink equal to the hole radius might produce a negative error of $0{\cdot}002q$. We are not aware of similar work at supersonic speeds.

Thermal creep effect.

In low density flow with Knudsen number greater than 0·1 the effect of thermal creep[15] should be considered if a temperature gradient exists along the pressure tube. The pressure measured at the cold end becomes smaller than the true pressure at the hot end the more so the greater the temperature ratio and the higher the Knudsen number. This is described[15] as being due to thermal circulation of the gas from the cold end along the tube wall and from the hot end in the tube centre. This effect might be modified at large Knudsen numbers by outgassing from the tube wall. In the present work the effect of thermal creep is negligible.

Turbulence effect.

Goldstein[16] states that in isotropic turbulence a static tube measures $p+\frac{1}{6}\rho u^2$ where u is the turbulent velocity. Fage[17] has shown that the reading S of a static tube and the true average pressure $\bar{p}$ may be related by $S = \bar{p}+k\rho[\bar{v}^2+\bar{w}^2]$ where v and w are the velocity components at right angles of the turbulence and ρ is the density. For a circular pipe $k = 0{\cdot}28$ and for a rectangular pipe $k = 0{\cdot}22$. Turbulence measurements in this tunnel have not so far been made.

APPENDIX C

Response of a Typical Model Lead to a Pressure Change.

Fig. 31 shows the response of various tubings to a step-change in pressure from atmospheric to vacuum. P.V.C. tubing was found to be better than rubber and the larger the internal diameter of the P.V.C. tubing the better the response. With rubber tubing the thicker the wall the better the response. Representative model leads made-up of a length of hypodermic tubing plus P.V.C. or tungum (copper alloy) tubing were also tested and the results are plotted in the upper part of Fig. 31. The profiles show a very rapid drop in pressure over the first few seconds, and the pressure range 20 to 80 mm *Hg* (normal starting vacuum in the working section) is reached in about 15 seconds. Therefore these curves may be used to estimate response times for normal tunnel running by subtracting 15 sec from the time indicated. For example lead 2 would take 2·5 minutes to reach a pressure of 1 mm *Hg*. Lead 3 however would require 1·25 minutes. This explains why the static pressure results at $p_0 = 300$ p.s.i.g., $M = 8{\cdot}6$ showed such a large scatter and were insensitive to condensation.

TABLE 1

Measurements of Condensation Onset.

Mach No.	Method	Perfect gas		Calorically imperfect (γ variable) thermally perfect ($pV = RT$)	
		P_∞	T_∞	P_∞	T_∞
		mm *Hg*	deg K	mm *Hg*	deg K
6·81	Static	4·69	47·1	4·69	47·1
6·86	Pressure	6·61	50·9	6·61	51·1
6·86		10·86	54·7	10·84	55·1
6·81	Pitot	4·69	50·6	4·69	50·7
6·86	Pressure	6·61	49·0	6·61	49·1
6·86		10·86	54·7	10·84	55·1
8·50	Pitot Pressure and	1·12	38·5	1·12	38·9
8·54	Thermocouple	1·78	42·0	1·76	42·7
8·59		2·55	43·5	2·51	44·2

TABLE 2

Estimates of Error in Measured Static Pressure at $M = 8{\cdot}57$.

p_0 (p.s.i.g.)	p_∞/q	$\Delta p/q$ units (all positive)			
		Total measured error	Hole size effect (Rayle)	Boundary layer displacements effect (F.P. form)	Other effects:— probe displacement turbulence, etc
300	0·0195	0·0069	0·0021	0·00235	0·00245
500	0·0195	0·0060	0·0021	0·00135	0·00255
750	0·0195	0·0053	0·0021	0·00085	0·00235

TABLE 3

Composition of Earth's Atmosphere (*Ref.* 21) (*Parts per million*)

Constituent	By volume	By weight
N_2	780,900	755,200
O_2	209,500	231,500
A	9,300	12,800
CO_2	300	460
Ne	18	12
He	5·2	0·72
CH_4	1·5	0·8
Kr	1	3
N_2O	0·5	0·8
H_2	0·5	0·04
O_3	0·4	0·7
Xe	0·08	0·4

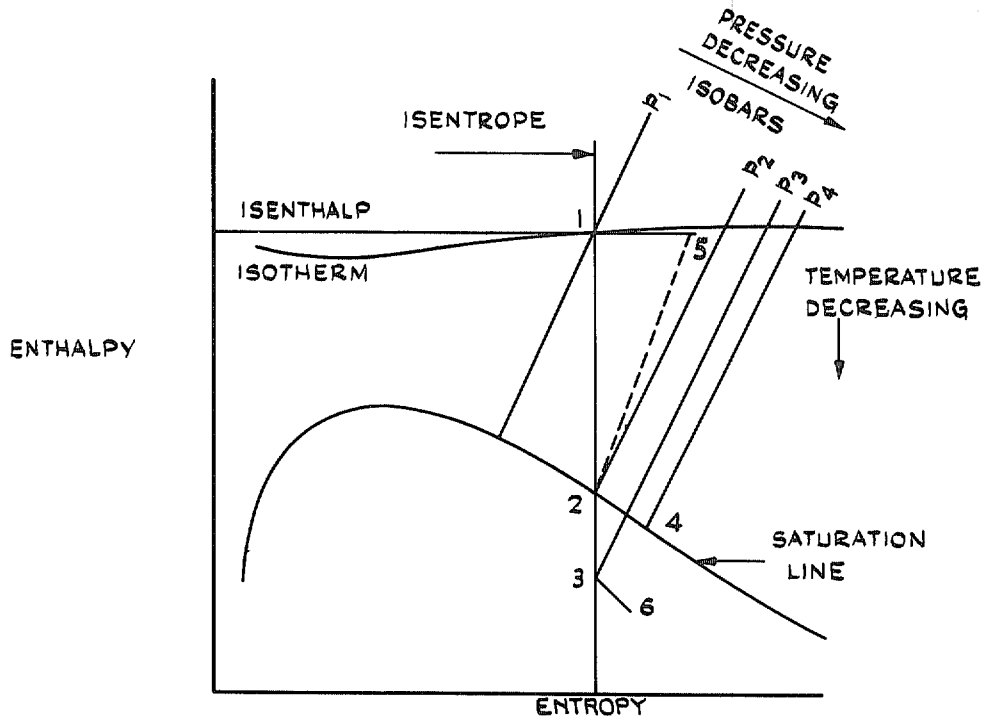

FIG. 1a. Mollier diagram for air.

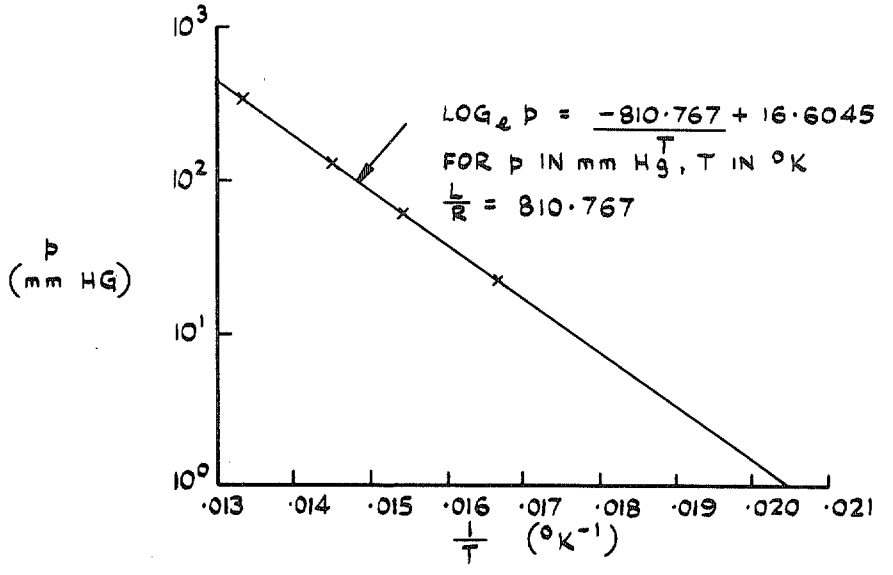

FIG. 1b. Condensation line of air from steady state experiments by Furukawa and McCoskey.

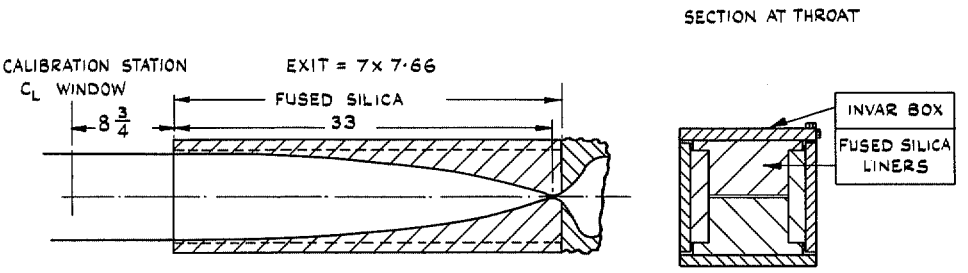

FIG. 2a. Two-dimensional nozzle (fused silica) $M = 6{\cdot}8$.

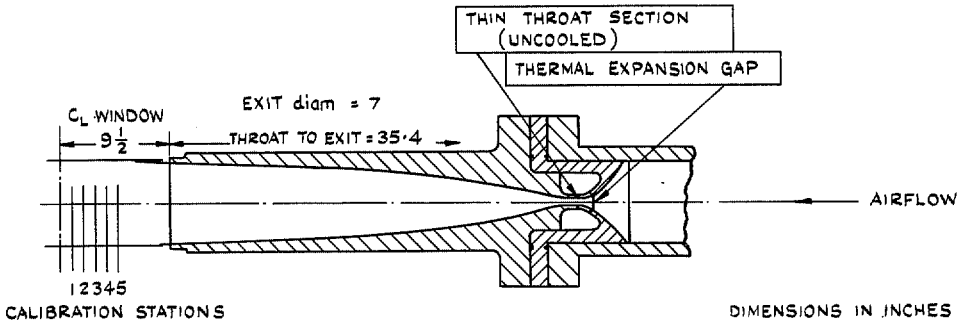

FIG. 2b. Axisymmetric nozzle (steel) $M = 8{\cdot}6$.

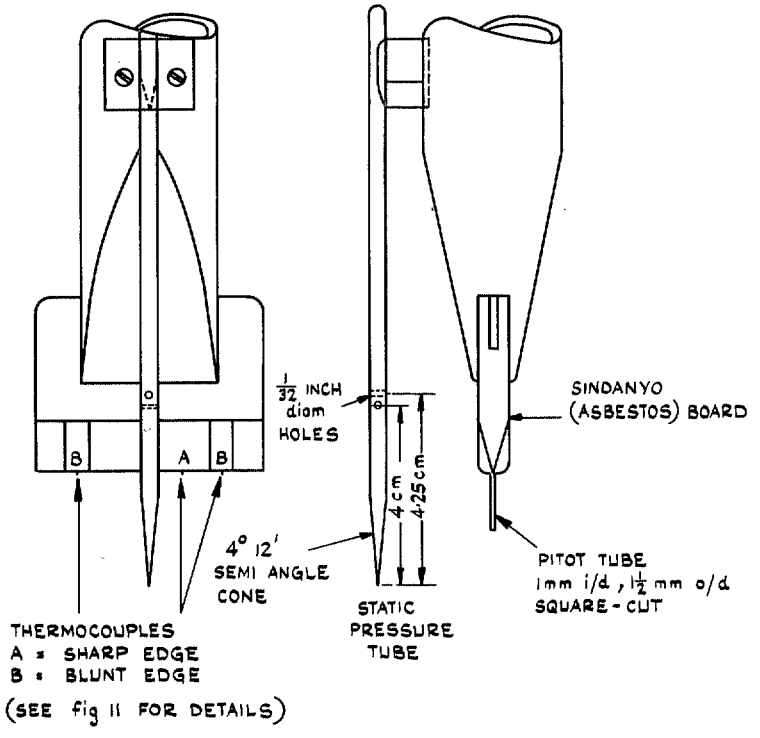

FIG. 3. Composite probe.

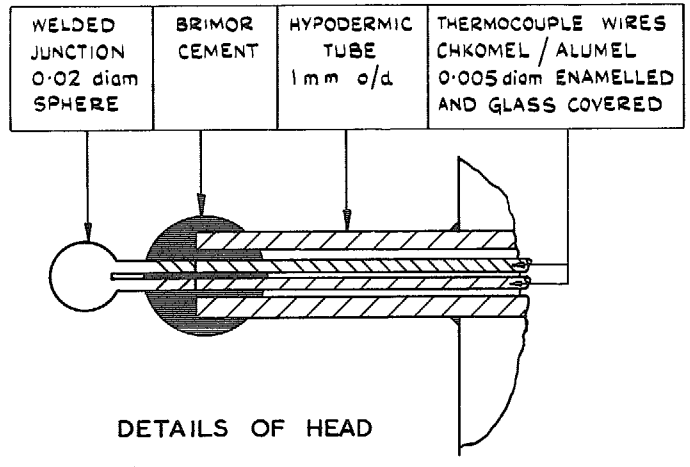

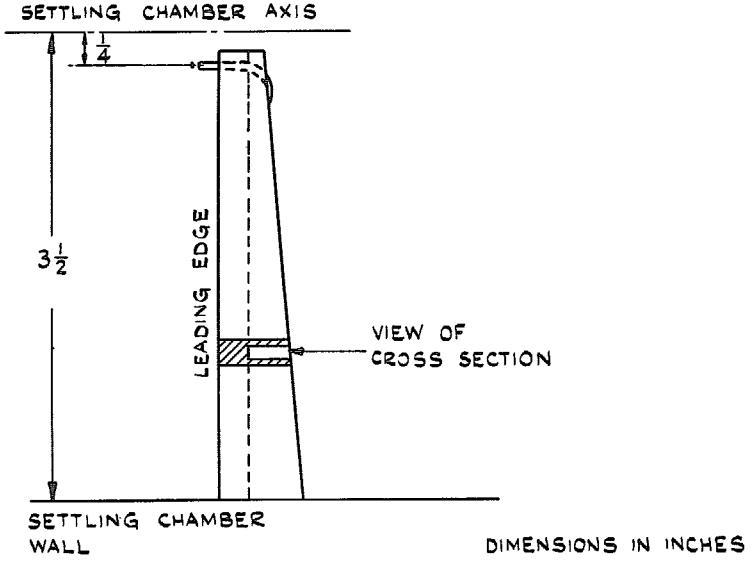

FIG. 4. Settling chamber total-temperature probe (principal features).

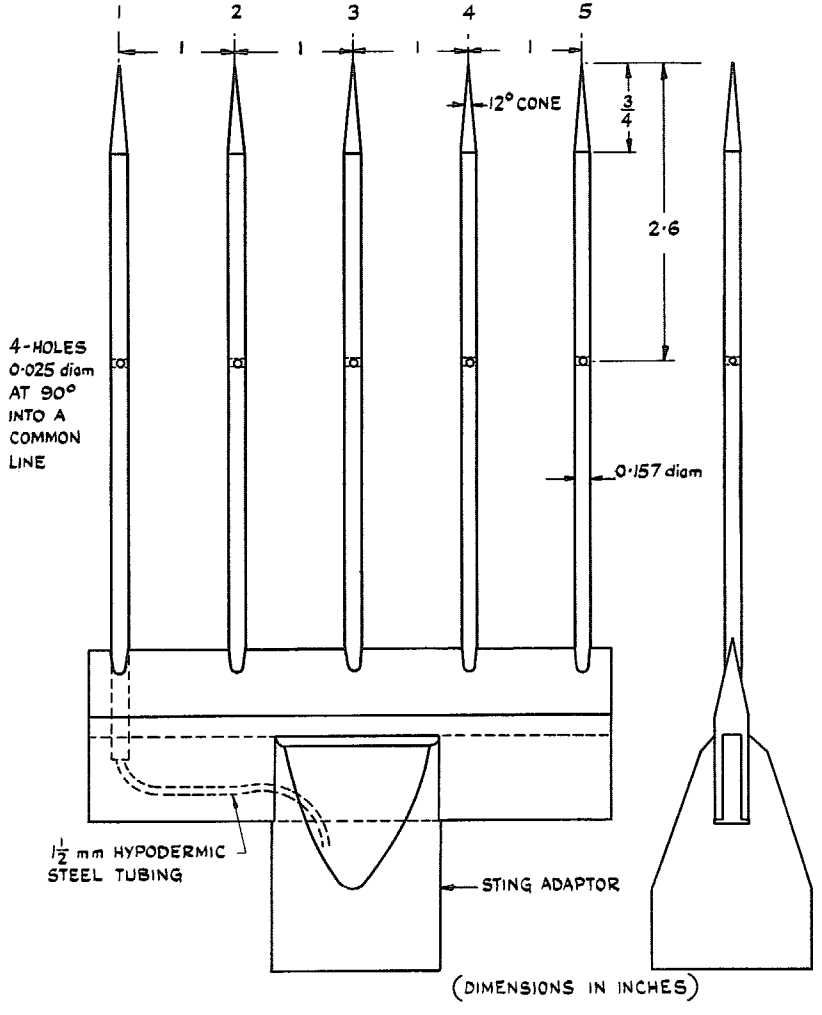

FIG. 5. Static-pressure rake.

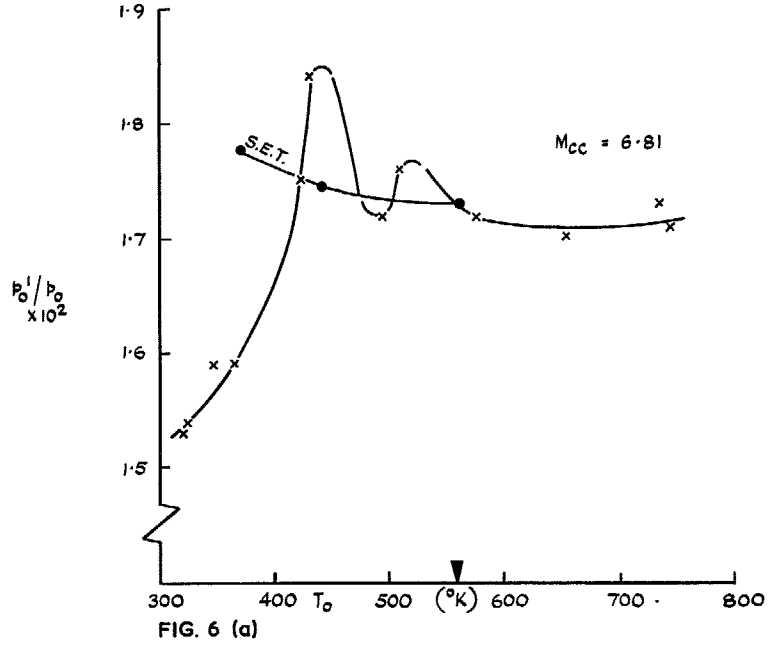

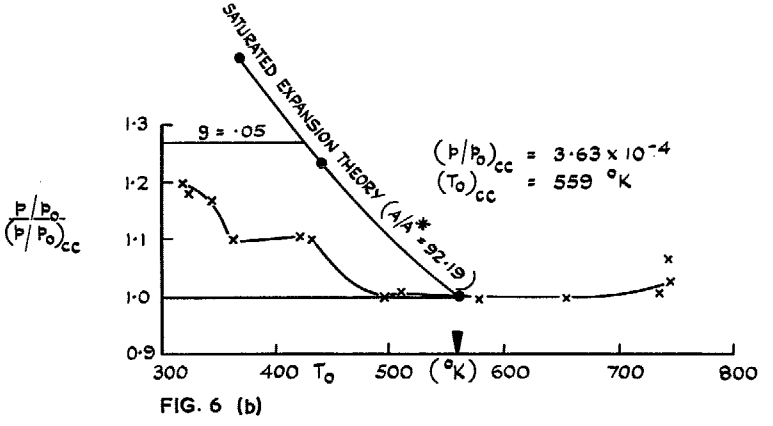

FIG. 6. Variation of (a) pitot pressure and (b) static pressure with T_0 at $M = 6{\cdot}8$ and $p_0 = 300$ p.s.i.g.

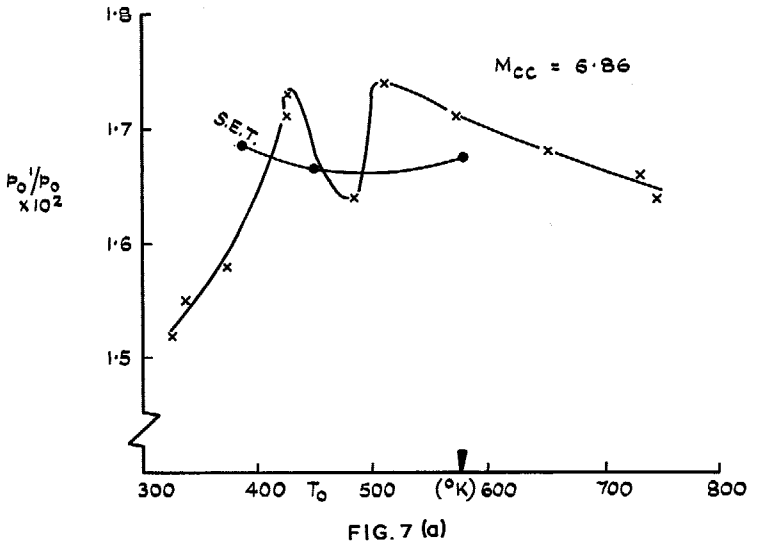

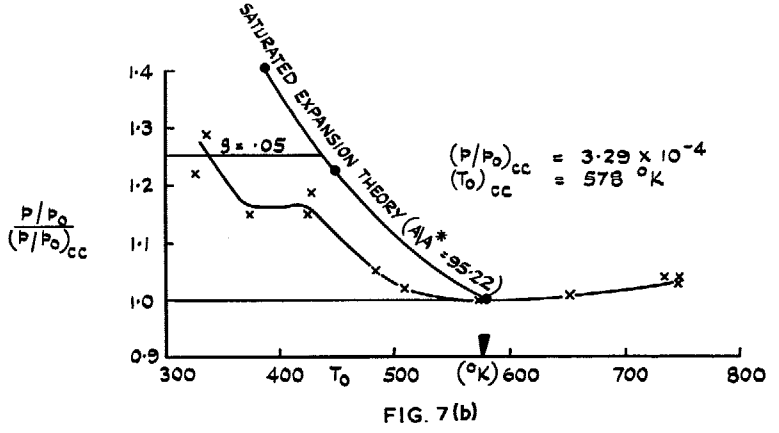

FIG. 7. Variation of (a) pitot pressure and (b) static pressure with T_0 at $M = 6{\cdot}8$ and $p_0 = 450$ p.s.i.g.

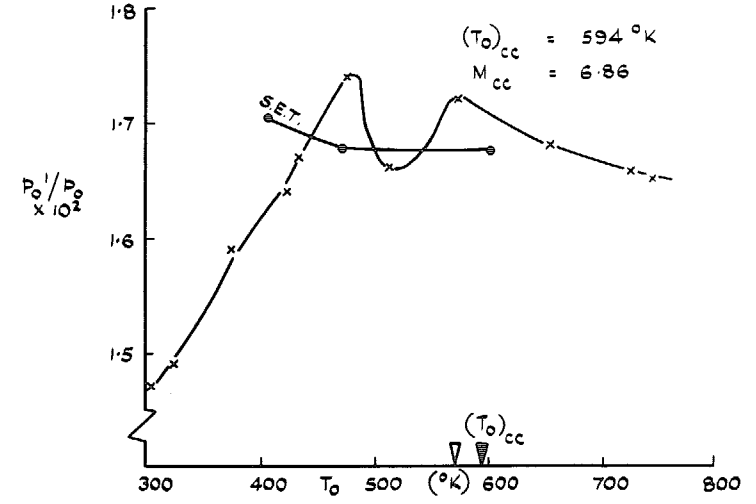

FIG. 8 (a)

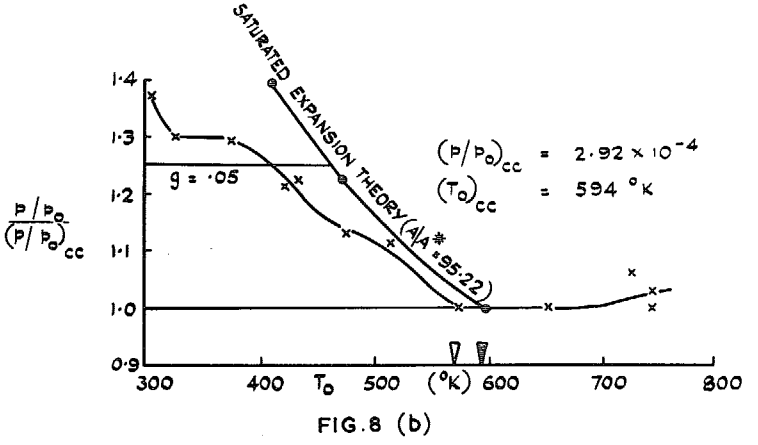

FIG. 8 (b)

FIG. 8. Variation of (a) pitot pressure and (b) static pressure with T_0 at $M = 6{\cdot}8$ and $p_0 = 750$ p.s.i.g.

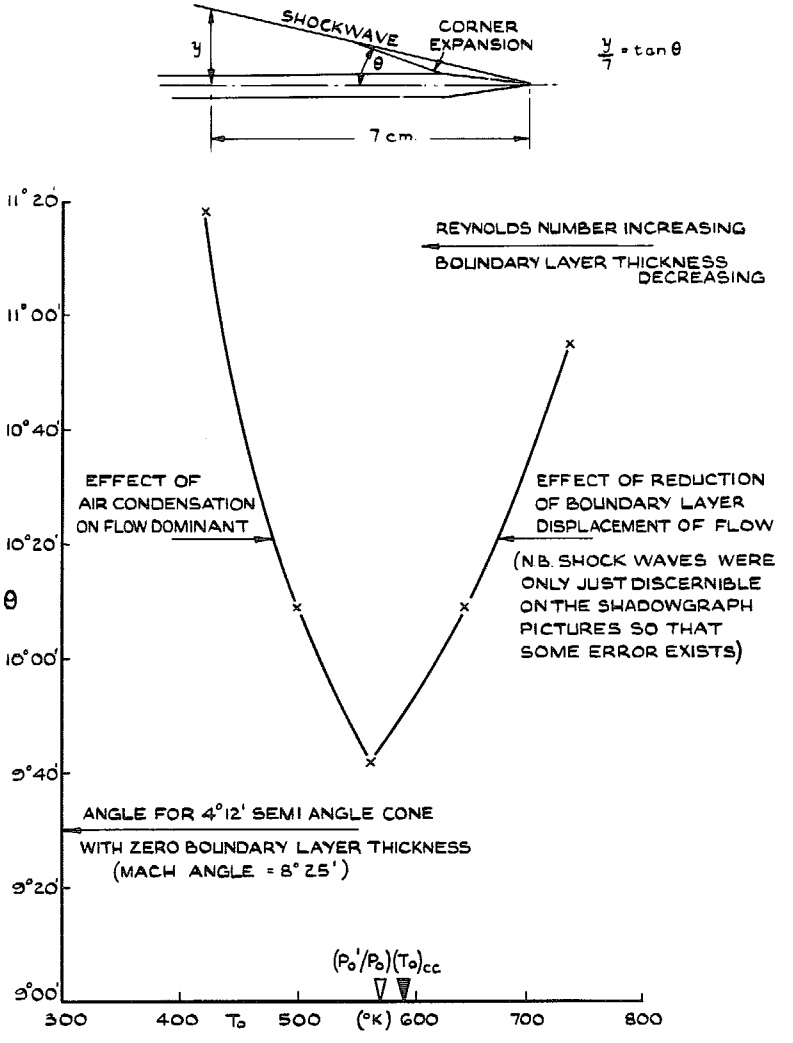

FIG. 9. Variation in angle of shockwave from tip of static probe at $M = 6{\cdot}86$ $p_0 = 750$ p.s.i.g.

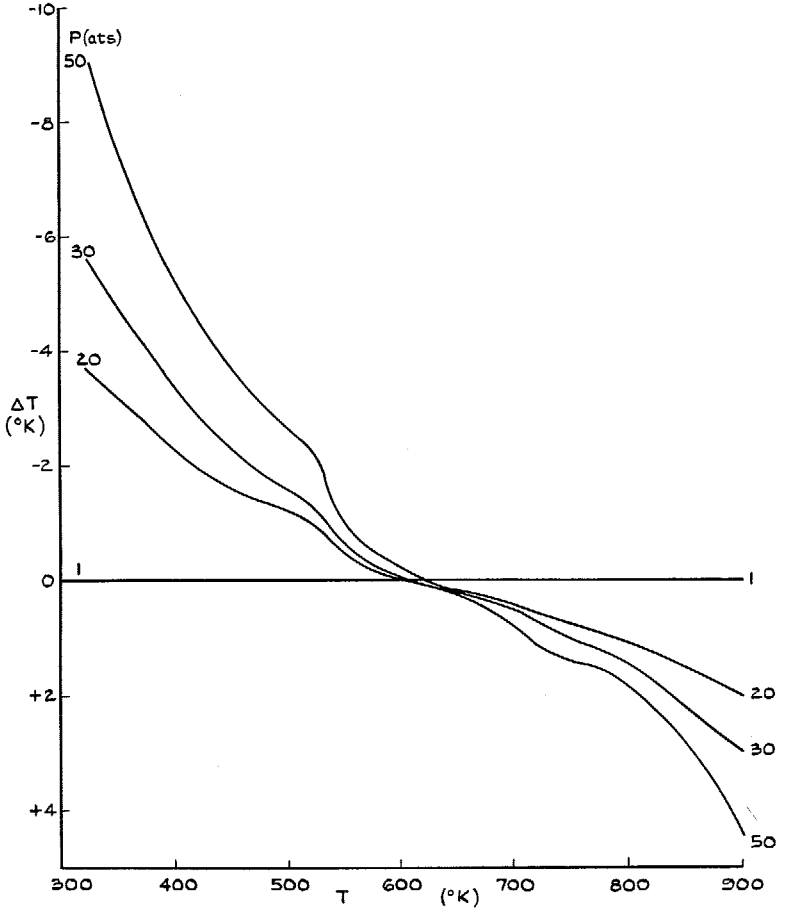

FIG. 10. Change in total temperature of air on expansion adiabatically to atmospheric pressure.

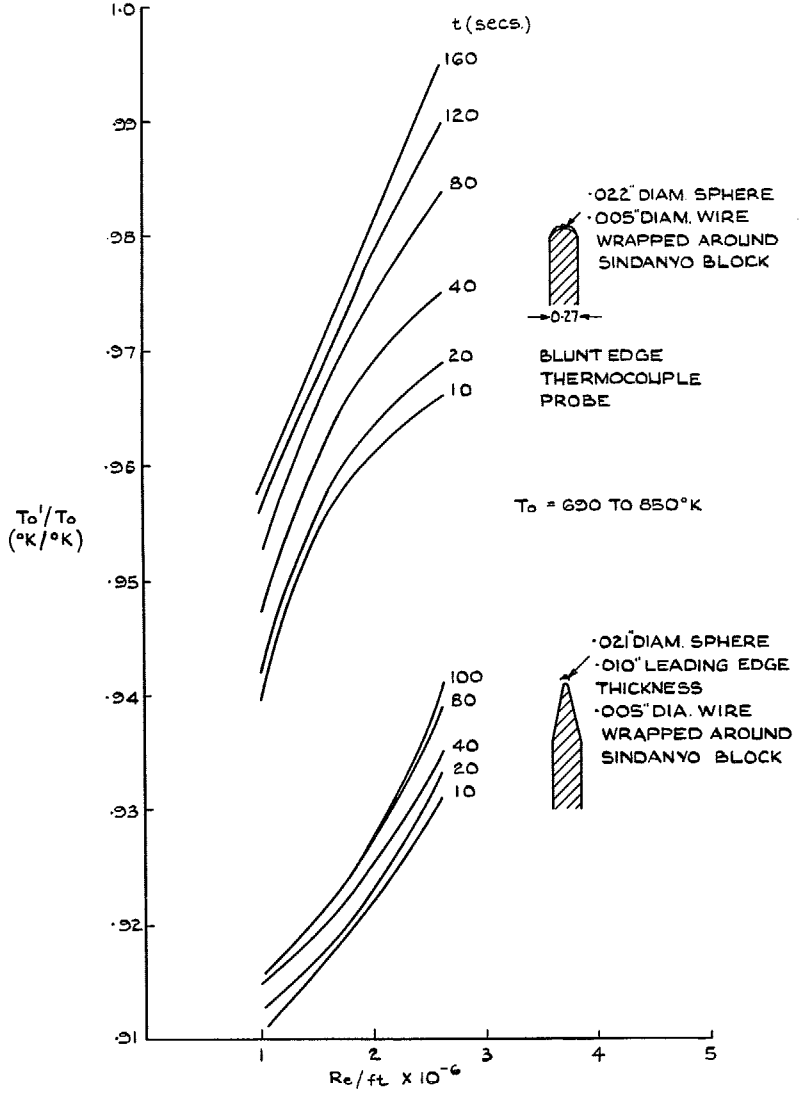

FIG. 11. Variation of recovery factor of thermocouple probes with time and Reynolds number per foot.

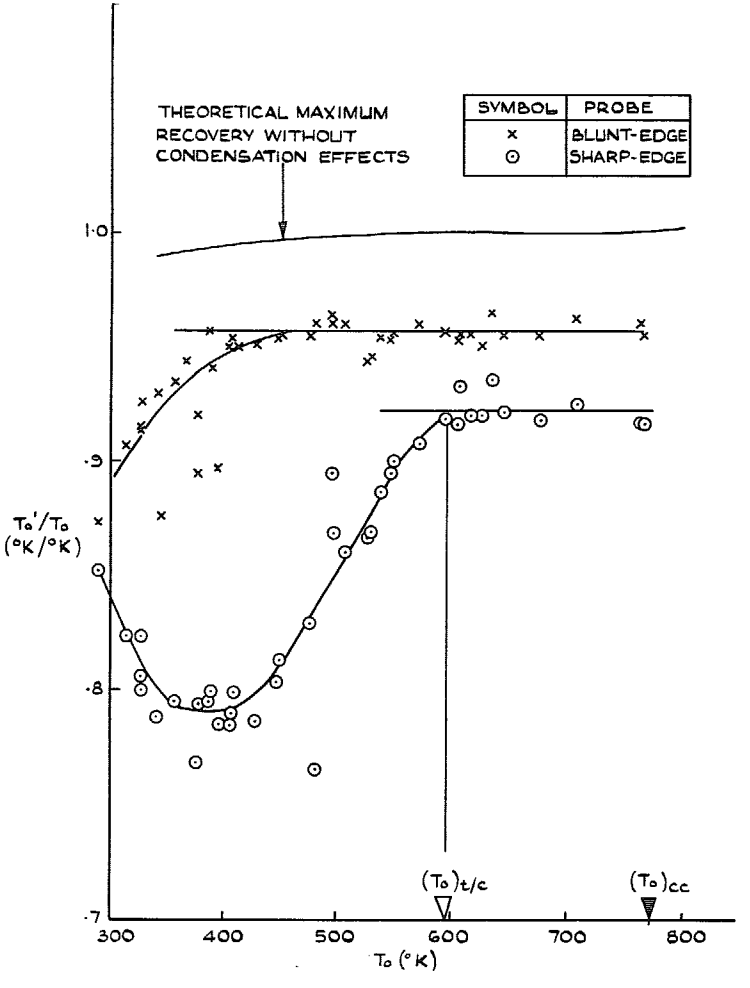

FIG. 12a. Variation of recovery temperature of thermocouple probes with T_0 at $p_0 = 300$ p.s.i.g. and $t = 80$ sec $M = 8{\cdot}6$.

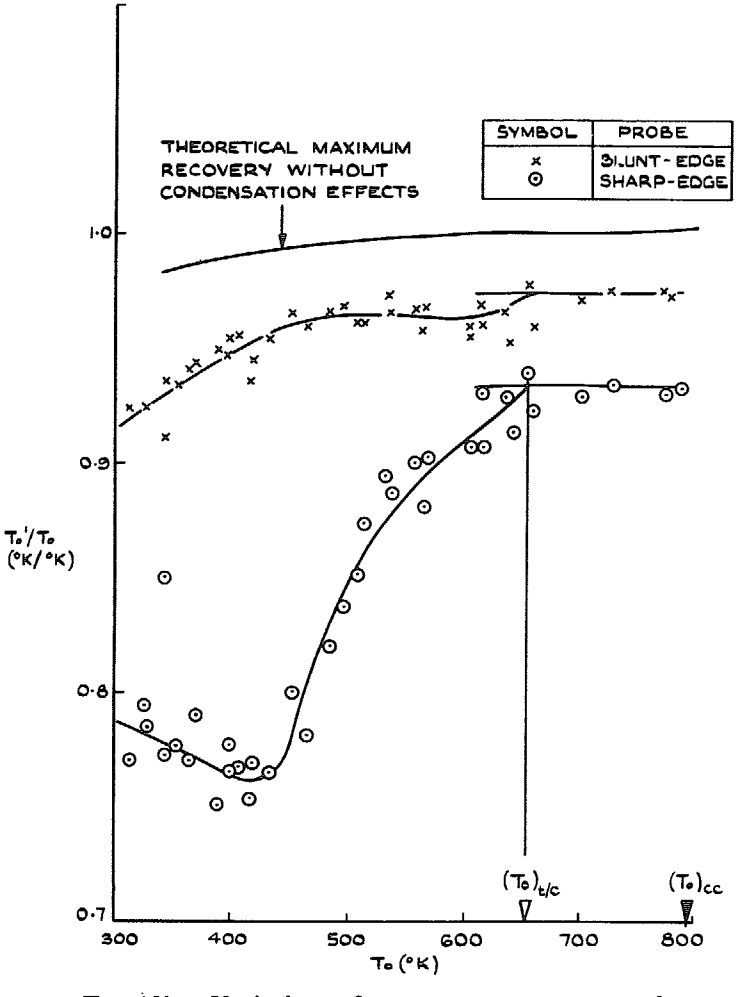

FIG. 12b. Variation of recovery temperature of thermocouple probes with T_0 at $p_0 = 500$ p.s.i.g. and $t = 80$ sec $M = 8{\cdot}6$.

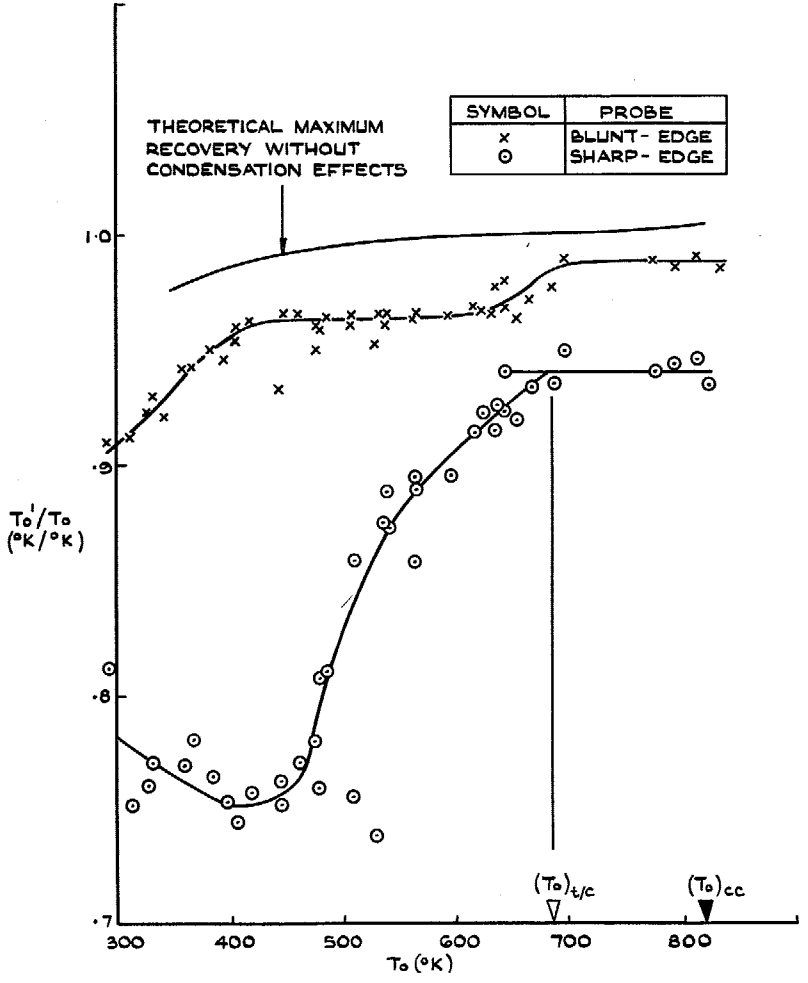

FIG. 12c. Variation of recovery temperature of thermocouple probes with T_0 at $p_0 = 750$ p.s.i.g. and $t = 80$ sec $M = 8{\cdot}6$.

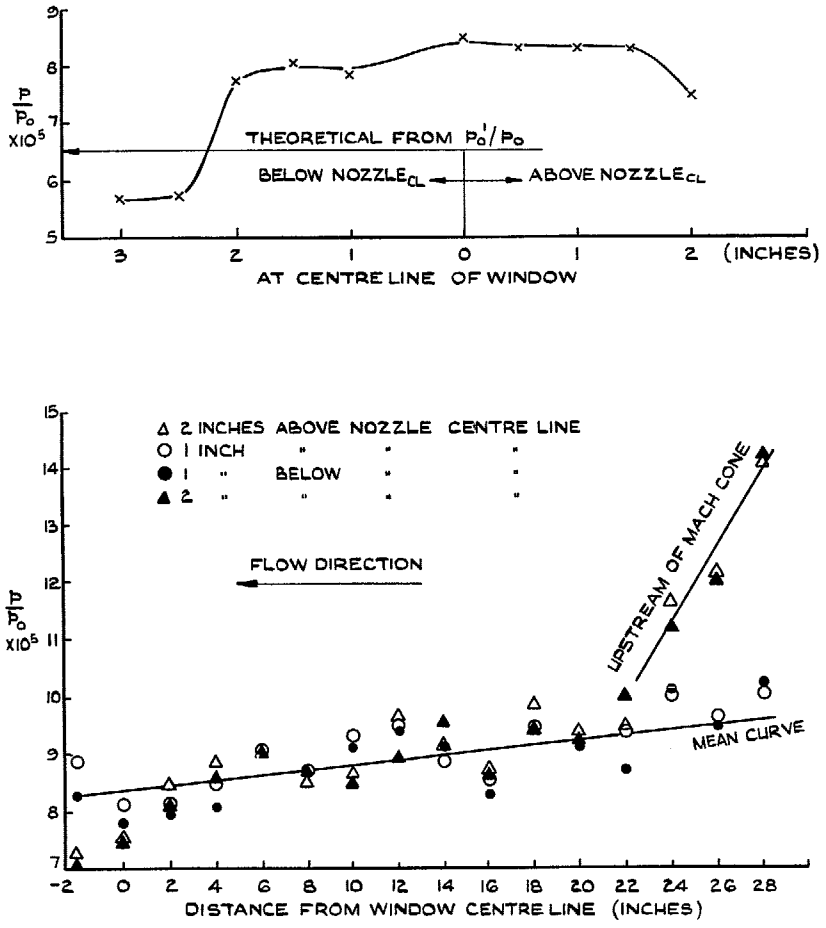

FIG. 13. Static-pressure measurements at $M = 8{\cdot}6$, $p_0 = 750$ p.s.i.g., $T_0 \simeq 830$ deg K.

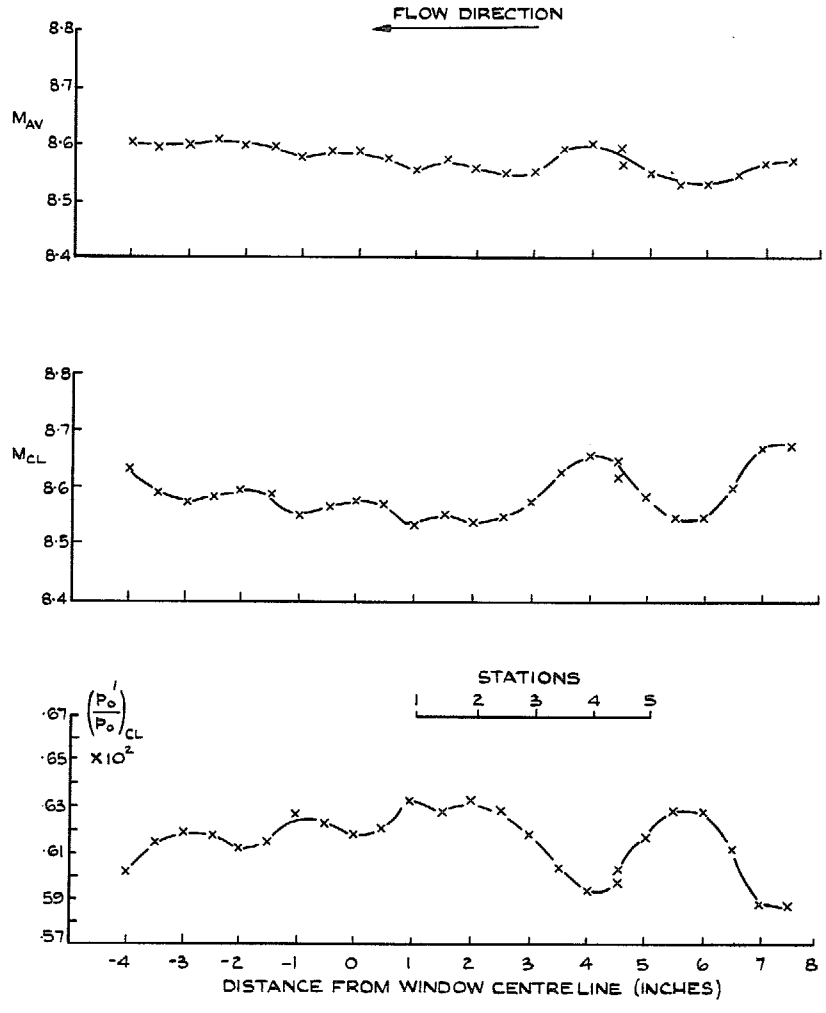

FIG. 14. Longitudinal calibration in subsaturated flow. (p_0 = 750 p.s.i.g., $T_0 > 820$ deg K).

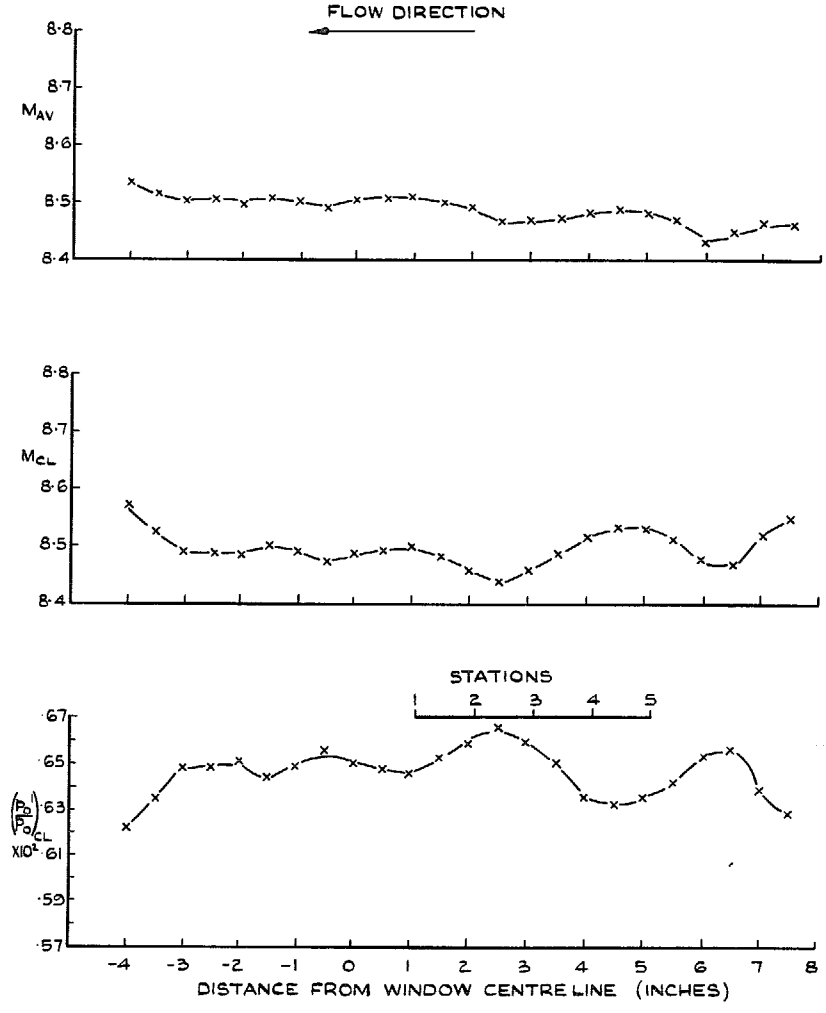

FIG. 15. Longitudinal calibration in supersaturated flow. (p_0 = 300 p.s.i.g., $T_0 \simeq 730$ deg K).

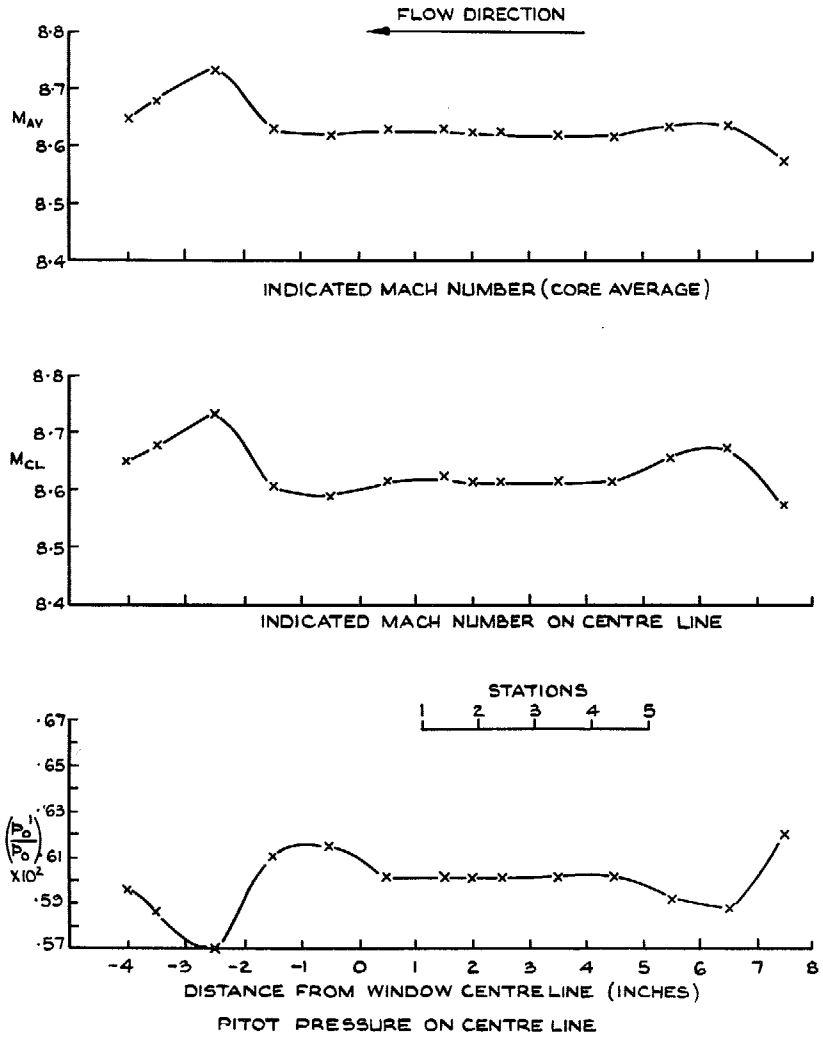

FIG. 16. Longitudinal calibration in condensing flow. (p_0 = 750 p.s.i.g., $T_0 \simeq$ 520 deg K).

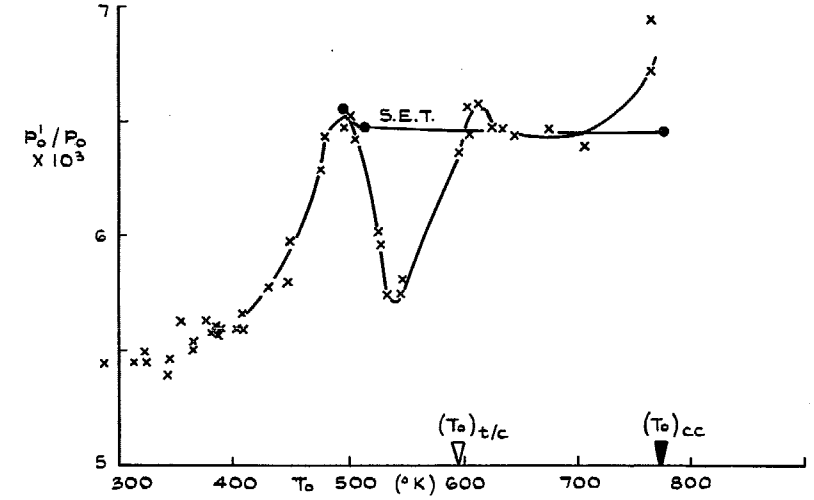

FIG. 17(a) AT STATION 5, r = 0

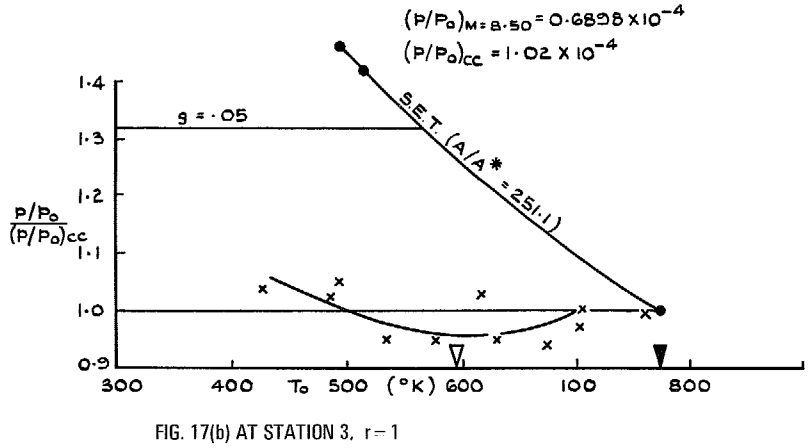

FIG. 17(b) AT STATION 3, r = 1

FIG. 17. Variation of (a) pitot pressure and (b) static pressure with T_0 at M = 8·6 and p_0 = 300 p.s.i.g.

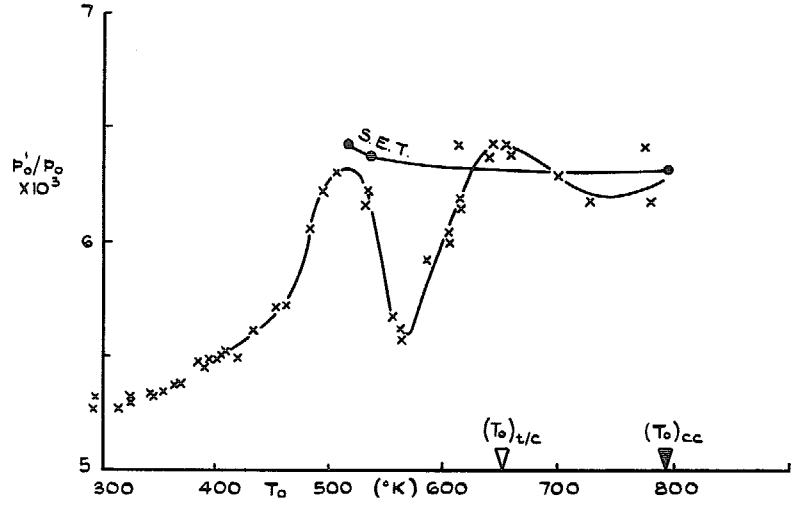

FIG. 18 (a) AT STATION 5, r = 0

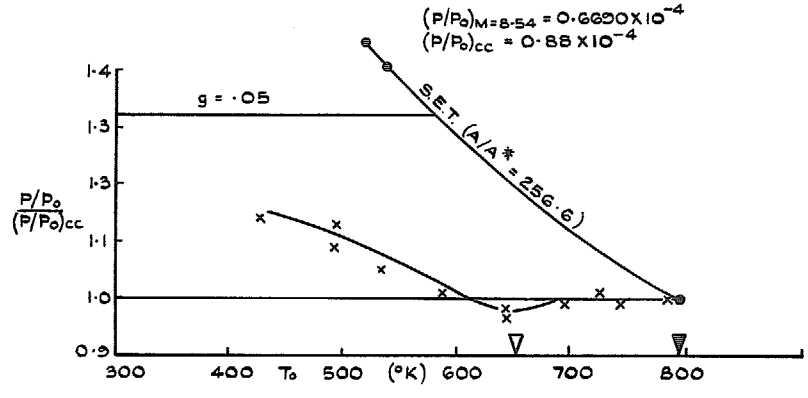

FIG. 18 (b) AT STATION 3, r = 1

FIG. 18. Variation of (a) pitot pressure and (b) static pressure with T_0 at $M = 8{\cdot}6$ and $p_0 = 500$ p.s.i.g.

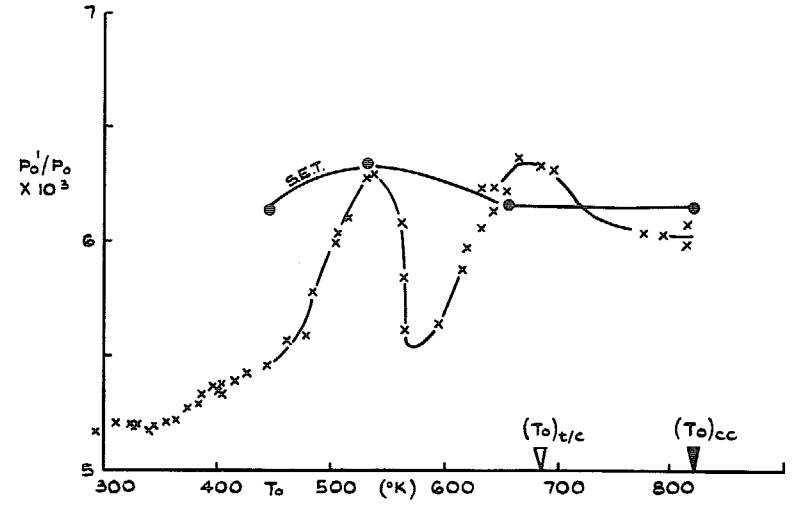

FIG. 19 (a) AT STATION 5, r = 0

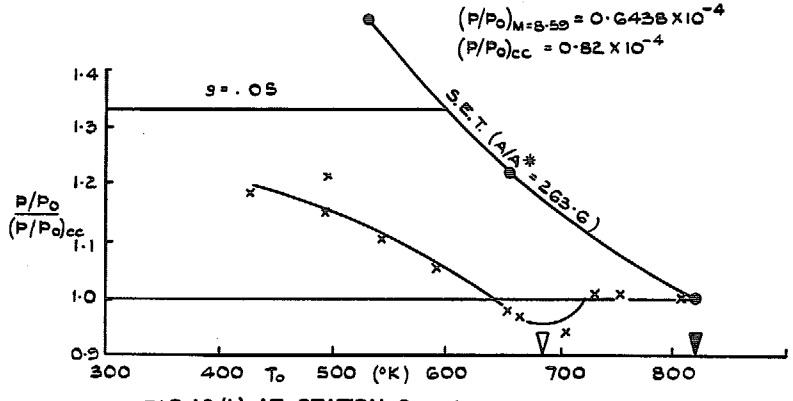

FIG. 19 (b) AT STATION 3, r = 1

FIG. 19. Variation of (a) pitot pressure and (b) static pressure with T_0 at $M = 8{\cdot}6$ and $p_0 = 750$ p.s.i.g.

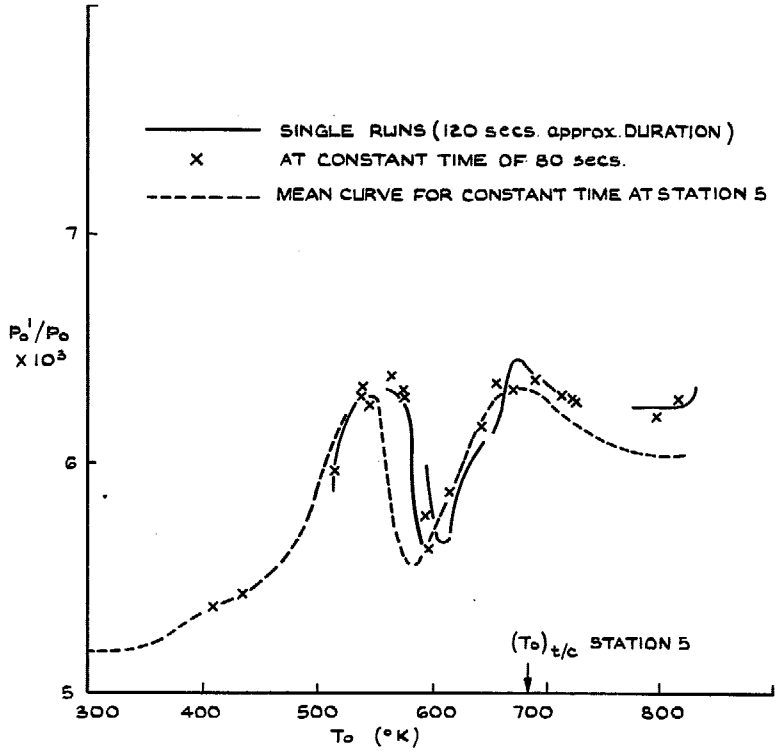

FIG. 20. Variation of pitot pressure (on centreline at Station one) with time (single runs) and with T_0 (constant time) at $p_0 = 750$ p.s.i.g.

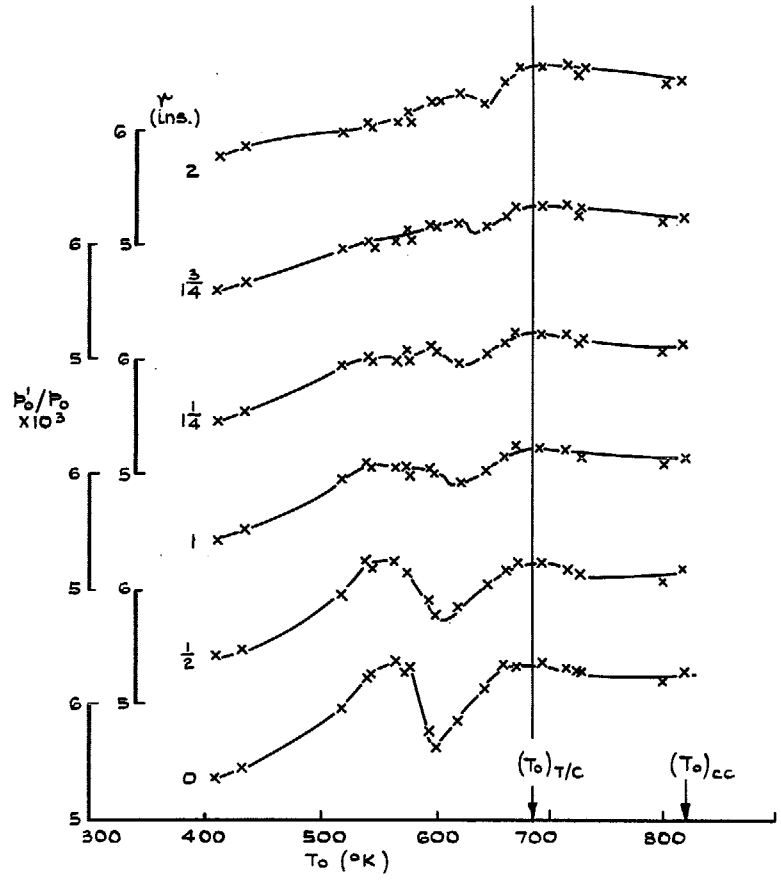

FIG. 21. Variation of pitot pressure with T_0 at different radii across the core ($t = 80$ sec) $M = 8{\cdot}6$ $p_0 = 750$ p.s.i.g. at Station 1.

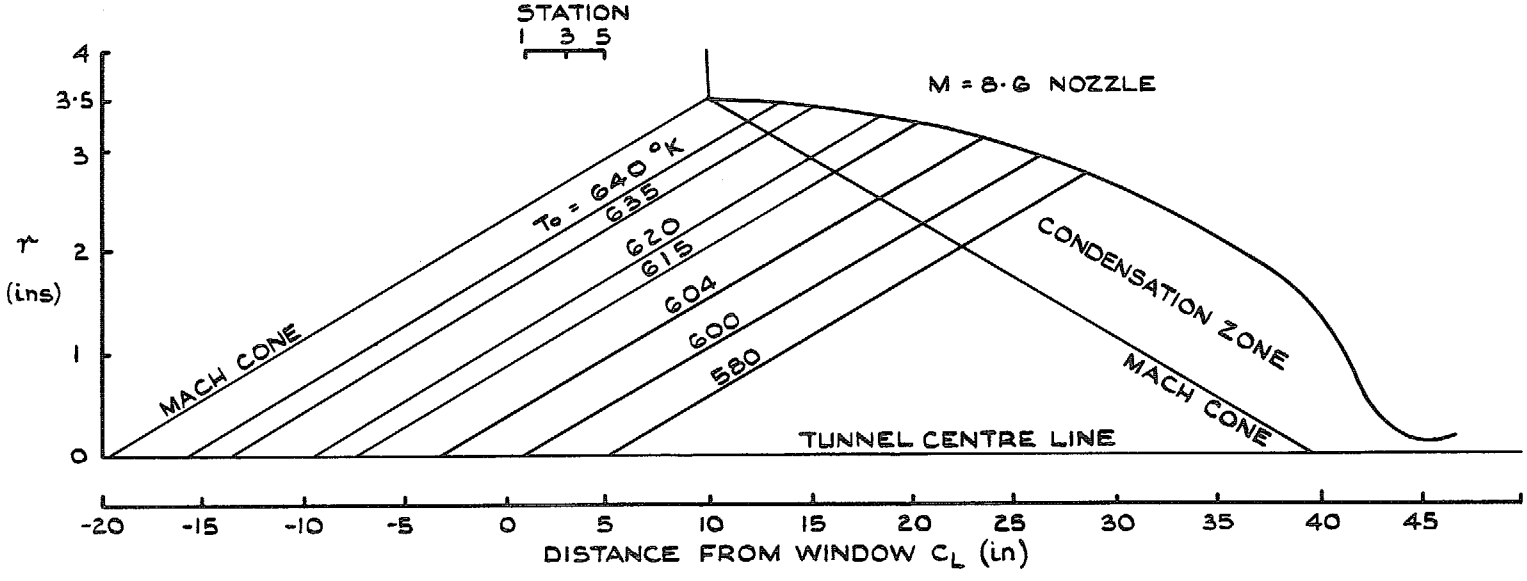

FIG. 22. Variation with temperature of the location of the recompression – field wavefront indicated by pitot-pressure profiles at $p_0 = 750$ p.s.i.g.

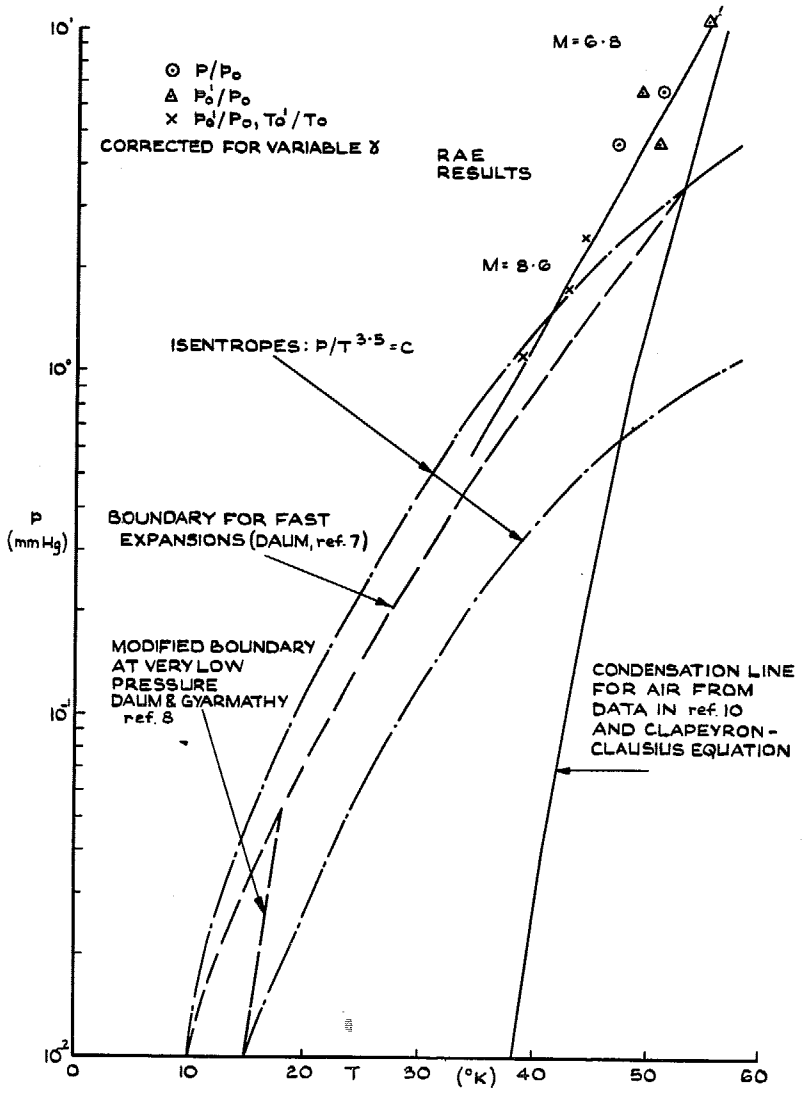

FIG. 23. R.A.E. results compared with Daum line and Clapeyron-Clausius line.

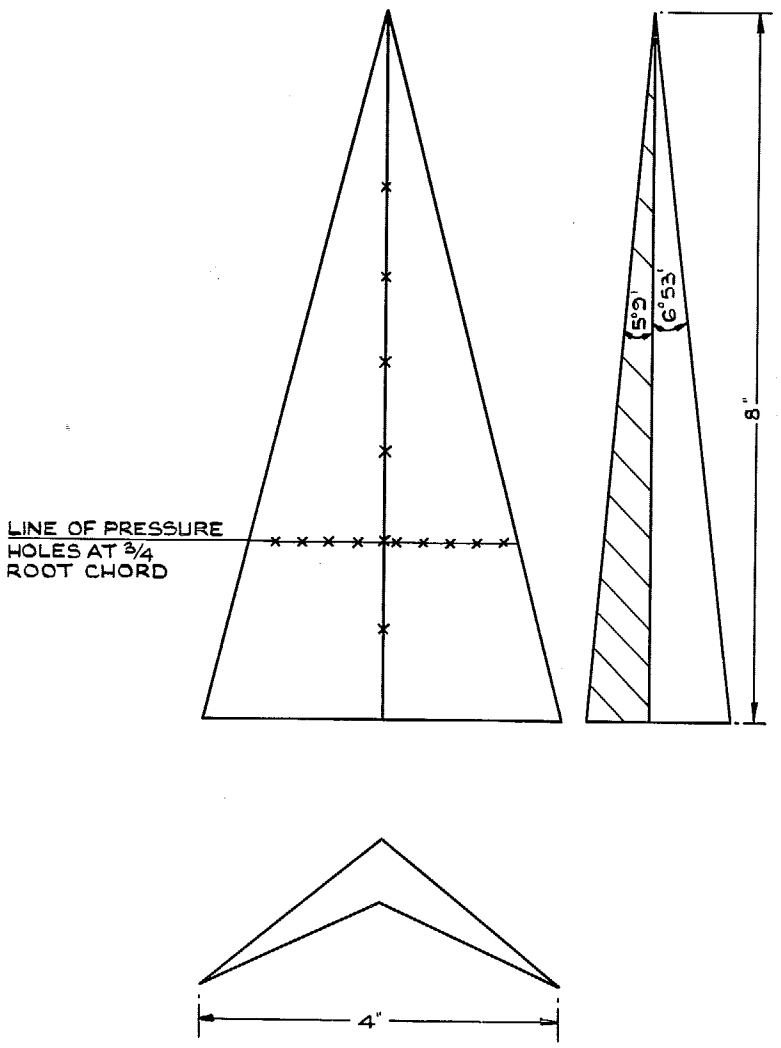

FIG. 24. Nonweiler delta model.

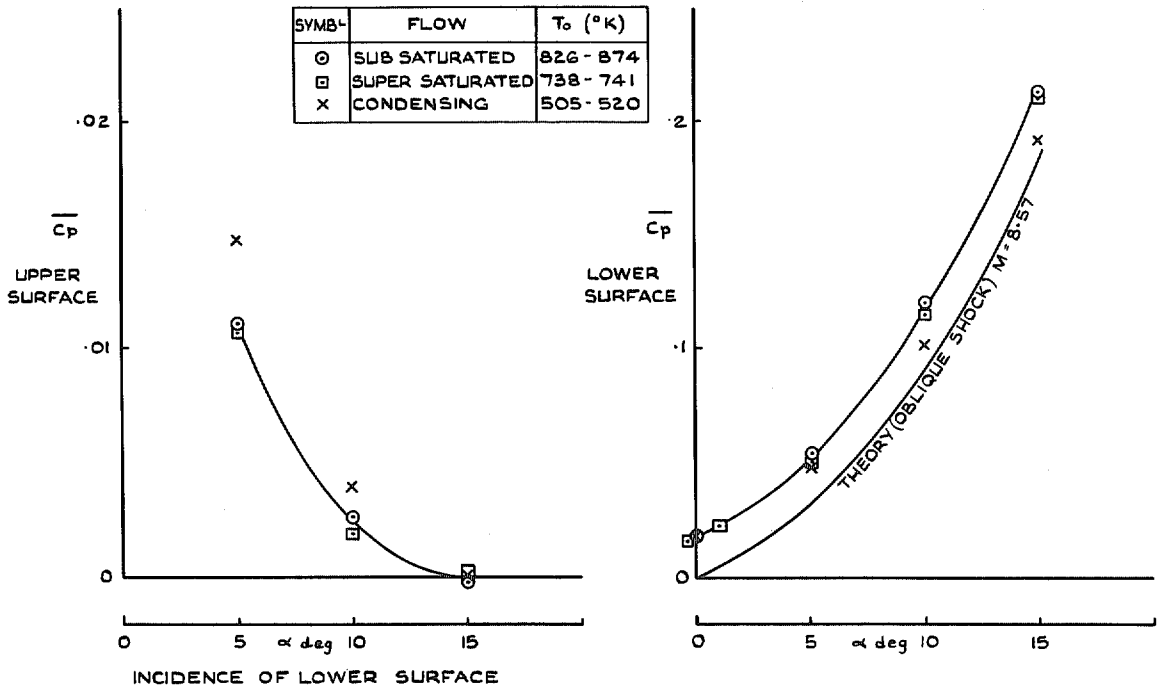

FIG. 25. Average pressure coefficients measured on a caret delta wing. $M = 8{\cdot}57$ and $p_0 = 750$ p.s.i.g.

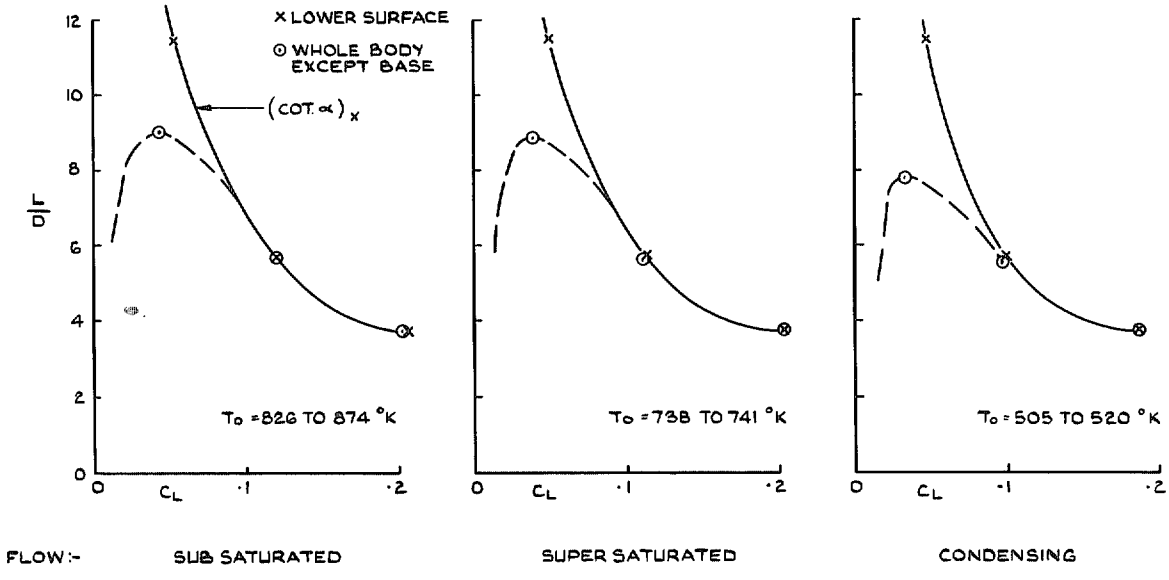

FIG. 26. Lift – drag ratios from measured pressures on a caret delta wing at $M = 8{\cdot}57$ and $p_0 = 750$ p.s.i.g.

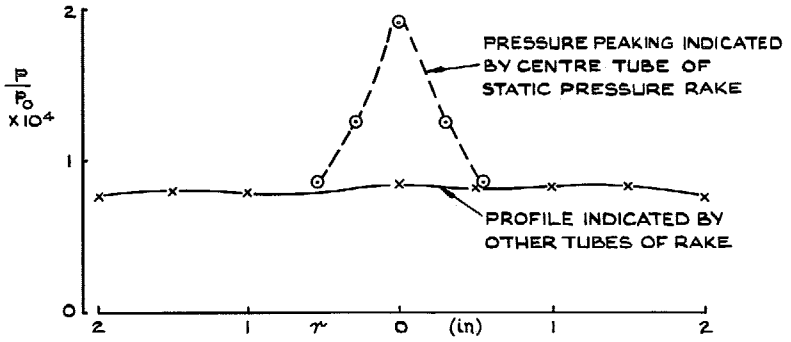

FIG. 27a. Measured profiles of static pressure without shields.

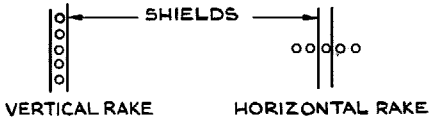

FIG. 27b. Shield arrangement.

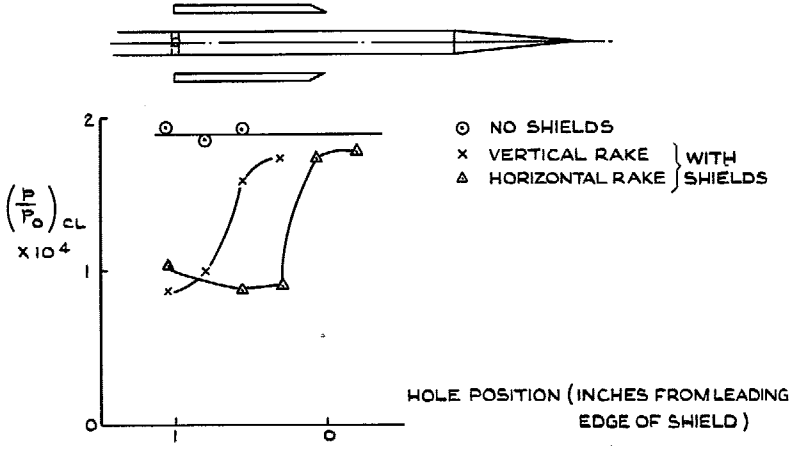

FIG. 27c. Influence of shields on centre tube.

FIG. 27. The effects of sting interference and shields on the pressure measured by the centre tube of the static pressure rake.

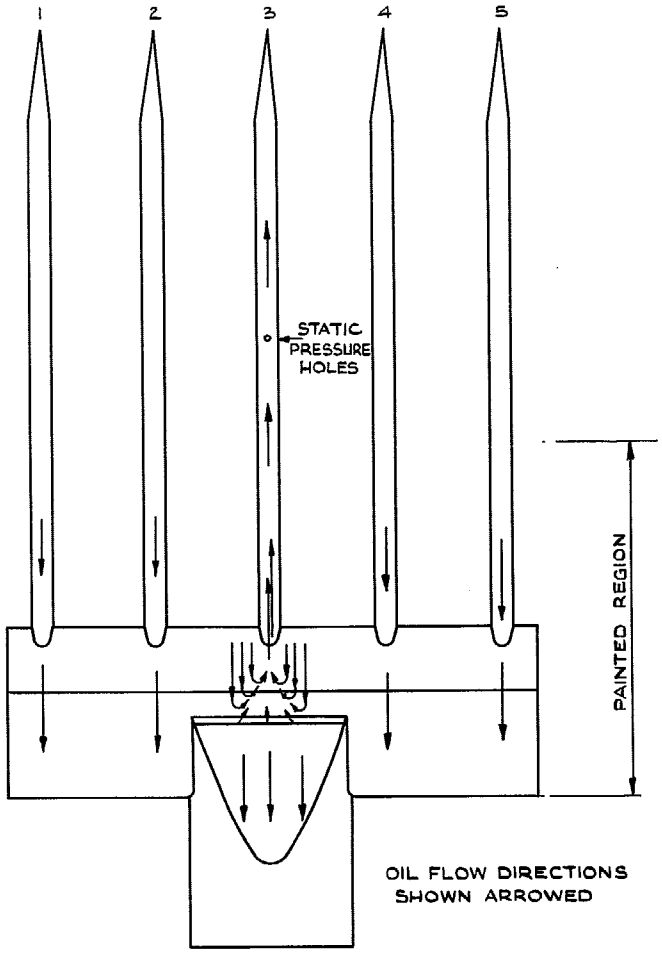

FIG. 28. Paint flow pattern on static-pressure rake using temperature-sensitive paint.

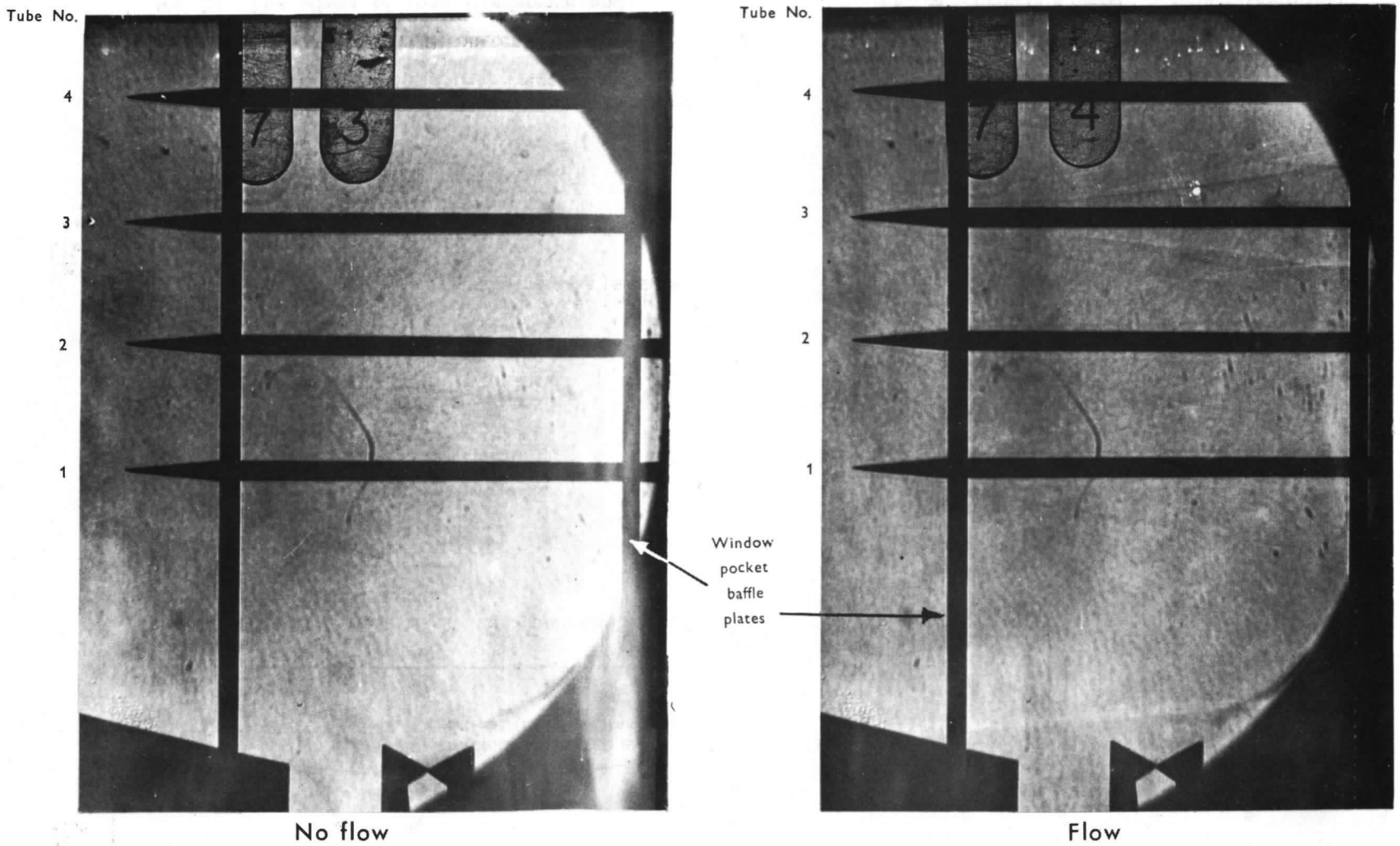

FIG. 29. Static pressure rake Fig. 5 in vertical position.
(Note the tremendous reach of the separation zone on No. 3 tube).

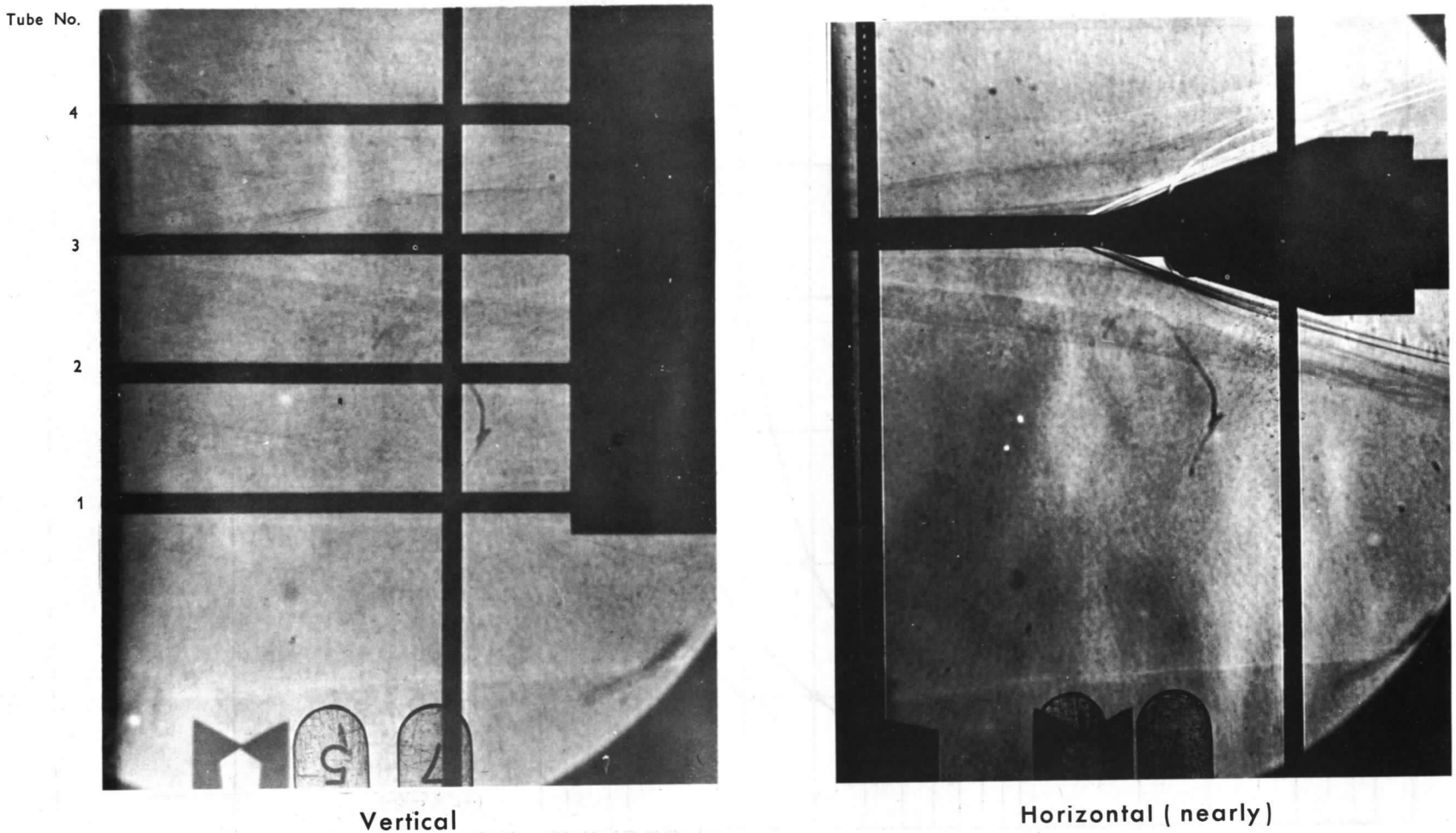

FIG. 30. Pictures of Flow at base of static pressure rake.
(n.b. large region of separated flow on No. 3 tube (centreline) due to sting).

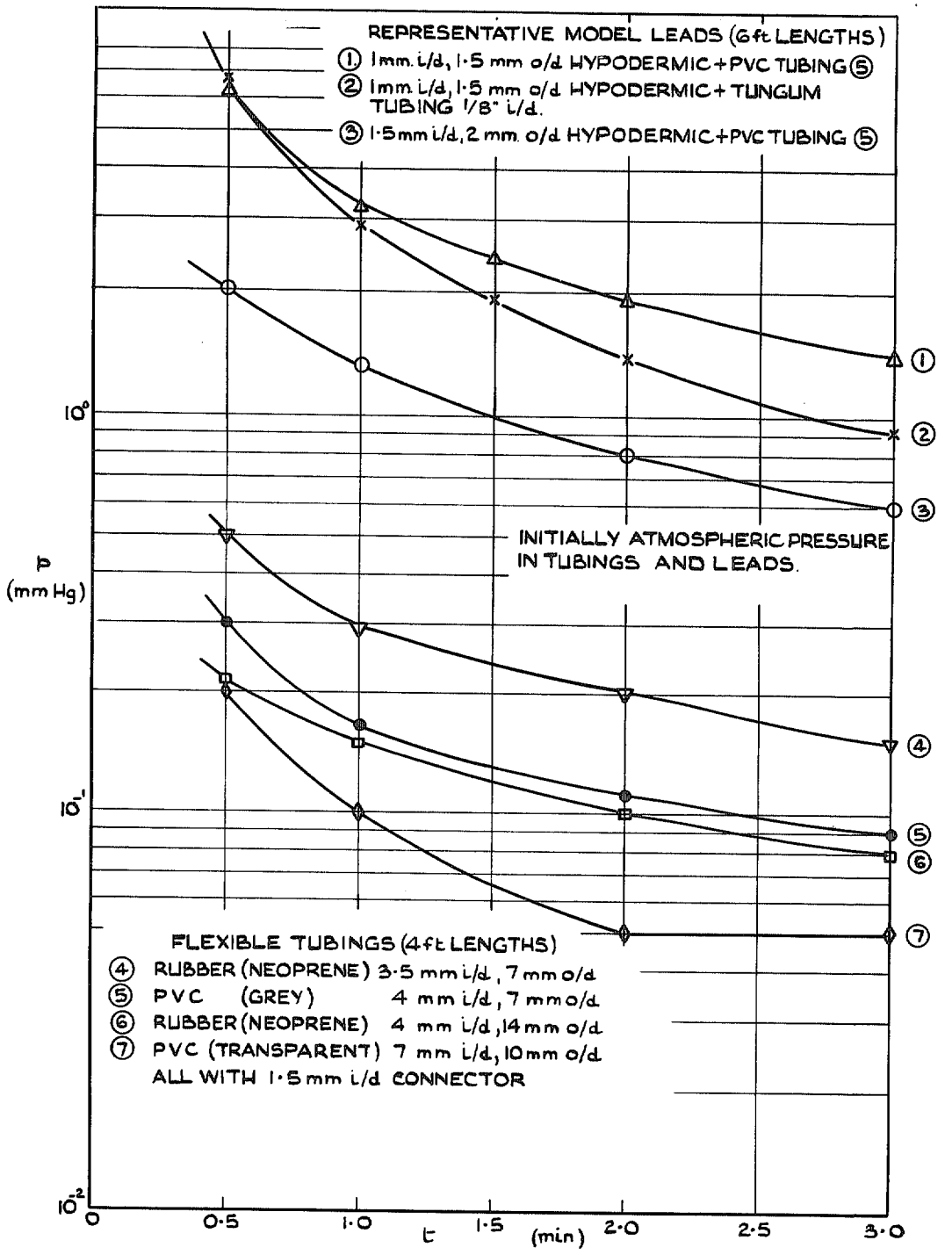

FIG. 31. The response of various tubings at low pressure.

Printed in Wales for Her Majesty's Stationery Office by Allens Printers (Wales) Limited.

Dd. 129527. K.5.

Published by
HER MAJESTY'S STATIONERY OFFICE

To be purchased from
49 High Holborn, London W.C.1
423 Oxford Street, London W.1
13A Castle Street, Edinburgh 2
109 St. Mary Street, Cardiff CF1 1JW
Brazennose Street, Manchester 2
50 Fairfax Street, Bristol 1
258–259 Broad Street, Birmingham 1
7–11 Linenhall Street, Belfast BT2 8AY
or through any bookseller

S.O. Code No. 23-3